

1 Slow-moving rock glaciers in marginal periglacial environment of

2 Southern Carpathians

3 Alexandru Onaca^{1,2}, Flavius Sîrbu², Valentin Poncoş³, Christin Hilbich⁴, Tazio Strozzi⁵, Petru Urdea^{1,2}
4 Răzvan Popescu⁶, Oana Berzescu², Bernd Etzelmüller⁷, Alfred Vespremeanu-Stroe⁶, Mirela Vasile⁸,
5 Delia Teleagă³, Dan Birtaş³, Iosif Lopătiță¹, Simon Filhol⁷, Alexandru Hegyi^{2,7}, Florina Ardelean¹
6

7 ¹Department of Geography, West University of Timișoara, Timișoara, Romania
8 ²Institute for Advanced Environmental Research, West University of Timișoara, Timișoara, Romania
9 ³Terrasigna, Bucharest, Romania
10 ⁴Department of Geosciences, University of Fribourg, Fribourg, Switzerland
11 ⁵Gamma Remote Sensing, Gumligen, Switzerland
12 ⁶Faculty of Geography, University of Bucharest, Bucharest, Romania
13 ⁷Department of Geosciences, University of Oslo, Oslo, Norway
14 ⁸Division of Earth, Environmental and Life Sciences, University of Bucharest Research Institute, Bucharest, Romania
15 *Correspondence to:* Flavius Sîrbu (flavius.sirbu@e-uvr.ro)

16 **Abstract.** Rock glaciers, composed of debris and ice, are widely distributed across cold mountain regions worldwide. Although
17 research on rock glaciers is gaining momentum, the distinct behaviour of rock glaciers in the marginal periglacial environments
18 remains poorly understood. This study combines remote sensing and in situ methods to characterize transitional rock glaciers in
19 the Carpathian Mountains. We used Persistent Scatterer Interferometry (PSInSAR) on Sentinel-1 images (2015 - 2020) to detect
20 slope movements associated with rock glaciers and differential GNSS measurements (2019-2021) to track horizontal movement
21 of 25 survey markers. Continuous ground temperature and winter snow cover bottom temperature (BTS) measurements
22 examined energy exchange fluxes affecting these rock glaciers. Geophysical surveys (electrical resistivity tomography and
23 refraction seismic tomography), and petrophysical joint inversion (PJI) quantified ice content in one rock glacier. PSInSAR
24 identified 92 moving areas (MAs) with slow displacement ($< 5 \text{ cm yr}^{-1}$) mostly between 2000 and 2300 meters, where solar
25 radiation was minimal. Near-surface thermal data from four rock glaciers suggest favourable conditions for permafrost
26 persistence, largely driven by internal ventilation processes (e.g., advection heat fluxes) throughout the winter. BTS confirmed
27 very low ground surface temperatures over much of the investigated rock glaciers, particularly in their upper parts and within
28 the MAs. Geophysical investigations reveal ice-poor permafrost remnants in the Galeșu rock glacier, while PJI modelling
29 estimated a low ground ice content ($\sim 18 \%$) in its upper sector. At this site, surface displacements stem from active layer
30 deformation, not permafrost creep. At two other sites, dGNSS markers moved consistently toward rock glacier fronts, indicating
31 permafrost creep. Regarding activity status, the majority of rock glaciers in the Retezat Mountains were categorized as relict,
32 with only 21% classified as transitional. Transitional rock glaciers occur 150 m higher and are slightly smaller than relict ones.

33 1. Introduction

34 Rock glaciers are prominent periglacial landforms, serving as indicators of permafrost presence at the time of their formation
35 (Haeberli et al., 2006). Formed by permafrost creep, they are debris-dominated features typically identified by their front, lateral
36 margins and occasionally ridge-and-furrow surface patterns (RGIK, 2023a). The geomorphic imprint of permafrost creep often
37 persist even after the ice within the rock glacier has completely melted (Kellerer-Pirklbauer et al., 2022). Most rock glaciers in
38 the Southern Carpathians are relict, though some retain isolated patches of permafrost (Vespremeanu-Stroe et al., 2012; Onaca
39 et al., 2013, 2015; Popescu et al., 2015, 2024). Indicators such as extensive lichen cover, vegetated fronts and the overall
40 morphological stability of many landforms suggest greatly reduced permafrost creep compared to pre-Holocene conditions

(Popescu et al., 2017). These rock glaciers are predominantly mantled by angular, coarse-grained blocks which facilitate ground cooling (Onaca et al., 2017a). The thermal offset associated with this blocky surface layer contributes to the maintenance of subzero temperatures in the subsurface over prolonged periods (Kellerer-Pirklbauer, 2019), supporting permafrost preservation even at lower altitudes (Colucci et al., 2019). Additionally, the 'chimney effect' - an advective heat flux process (Delaloye and Lambiel, 2005) - enhances surface cooling in highly porous, openwork structures.

Permafrost creep involves both the internal deformation of ice within the frozen material and shearing at discrete planes within or just beneath the frozen structure (Cicoira et al., 2021). Surface displacement may also result from active layer processes, such as solifluction, or block tilting and sliding, which can occur independently of permafrost creep (Serrano et al., 2010; Cicoira et al., 2021). Interest in rock glacier surface kinematics has grown recently (Kellerer-Pirklbauer et al., 2024; Kääb and Røste, 2024; Pellet et al., 2024; Hu et al., 2025) driven by the need to understand mountain permafrost response to climate change. While the response of rock glaciers to present-day air temperature rising is intricate in many instances, increased rock glacier velocities have been linked to warmer climate (Wirz et al., 2016; Cicoira et al., 2019; Kenner et al., 2019; Kääb et al., 2021; Marcer et al., 2021; Kellerer-Pirklbauer et al., 2024). Rising temperatures within frozen debris enhance movement rates, as warming reduces the viscosity of the ice and promotes additional lubrication from infiltrating water (Kääb et al., 2007). Annual horizontal surface velocities typically range from millimetres to a few meters (Strozzi et al., 2020), but destabilization can raise them above 10 m yr⁻¹ (Roer et al., 2008; Delaloye et al., 2013; Eriksen et al., 2018; Marcer et al., 2021; Hartl et al., 2023). Destabilization involves abrupt acceleration of a section of the rock glacier, often by up to two orders of magnitude, accompanied by surface features such as cracks, scarps, and crevasses reflecting enhanced internal strain between stable and unstable areas (Marcer et al., 2021; Hartl et al., 2023).

Satellite radar interferometry (InSAR) has proven effective for analysing rock glacier kinematics, detecting millimetre-scale motion (Liu et al., 2013; Necsoiu et al., 2016; Strozzi et al., 2020; Bertone et al., 2022). This technique enables the mapping of land surface deformation with an appropriate spatial and temporal resolution over vast areas (Bertone et al., 2022). Surface displacements can be attributed to permafrost creep only when flow direction and velocity are spatially consistent and uniform over a documented period (RGIK, 2023a). Permafrost creep generally requires an ice-rich core at least 10-25 m thick (Cicoira et al., 2021). In contrast, displacements in rock glaciers with thinner frozen debris are primarily driven by deformations within the active layer above the permafrost table.

Although rock glaciers in discontinuous permafrost have been widely studied, those in marginal periglacial environments have received far less attention (Serrano et al., 2010; Necsoiu et al., 2016). In such settings, rock glaciers exhibit significantly slower movement rates (a few cm yr⁻¹) and are often referred to as transitional rock glaciers (RGIK, 2023a), largely due to the high shear strength of the material, which inhibits fast creep movement (Cicoira et al., 2021). While slow-moving rock glaciers have been reported globally (Brencher et al., 2021; Bertone et al., 2022; Lilleøren et al., 2022; Lambiel et al., 2023), the relationship between their velocity and ground ice content was rarely addressed (Serrano et al., 2010). In remote, high-mountain environments where borehole data are scarce, petrophysical joint inversion (PJI) of seismic refraction and electrical resistivity offers a promising method to estimate ice content quantitatively (Wagner et al., 2019).

The Southern Carpathian range is a key region in Europe where transitional rock glaciers are studied. Enhanced continentality in this range induced a distinct pattern of periglacial phenomena compared to other mid-latitude mountains in Europe (Onaca et al., 2017a). In such marginal periglacial settings, permafrost is typically sporadic or patchy, with its distribution strongly influenced by local site conditions (Stiegler et al., 2014; Onaca et al., 2015; Kellerer-Pirklbauer, 2019; Popescu et al., 2024).

This study presents new insights into rock glacier kinematics and permafrost conditions in the Retezat Mountains, with a focus on understanding their behaviour in marginal periglacial settings. Specifically, we aim to: (i) identify and analyse moving areas using SAR-based persistent scatterers interferometry (PSInSAR); (ii) update the existing rock glacier inventory with kinematic data; (iii) estimate ground ice content through petrophysical joint inversion of electrical resistivity and seismic refraction data; and (iv) characterise the thermal conditions at the rock glaciers surface.

84 2. Study area

85 The Retezat Mountains, part of the Southern Carpathians (also known as the Transylvanian Alps), are among the highest massifs
86 in the Romanian Carpathians. Located in their western sector (45°22' N and 22°53' E), the range reaches elevations up to 2500
87 m, revealing a typical alpine landscape (Fig. 1). The region has a moderate temperate continental climate, classified as subarctic
88 or boreal under the Köppen system. At 2000–2100 m elevation, the mean annual air temperature is around 0° C, with annual
89 precipitation averaging 1000 mm (calculated for the period 1961-2007) (Onaca et al., 2017a). Compared to the 1961-1990
90 baseline, the 1991-2020 period was 0.8 °C warmer above 2000 m in the Southern Carpathians (Berzescu et al., 2025).

91 The Retezat Mountains span two major distinctive tectonic-structural units: the Danubian and Getic Domains, both forming part
92 of a thrust sheet system. The Danubian Domain, is dominated by two large granitic bodies—Retezat and Buta (Pavelescu, 1953)
93 —, which are bordered by epi- and meso-metamorphic schists of the Getic Nappe. Mesozoic rocks, especially limestones, are
94 common in the southern part of this mountain range (Urdea, 2000). Granite underlies 87 % of the rock glaciers in the Retezat
95 Mountains (Fig. 2), while the remaining landforms are situated on metamorphic schists.

96 The Retezat Mountains boast one of the most extensive and diverse assemblages of glacial and periglacial landforms in the
97 Romanian Carpathians. Notably, they host the largest glacial cirques in the region, which together cover about. 8 % of the
98 massif's area (Urdea, 2000). During the Last Glacial Maximum (LGM) (20.6 ka), glaciers descended to elevations as low as
99 1000-1300 m (Ruszkiczay-Rüdiger et al., 2021). Five deglaciation phases followed during the Late Glacial, but no glacial
100 advance has been recorded in the central Retezat since the Younger Dryas, based on cosmic-ray exposure dating (Ruszkiczay-
101 Rüdiger et al., 2021).

102 Rock glaciers likely began forming during the Younger Dryas, and have mostly become relict or transitional since the Holocene.
103 Permafrost associated with rock glaciers was first documented in 1993 in this mountain range (Urdea, 1993). A recent inventory
104 identified the Retezat Mountains as having the highest number (94) and density (0.52 landforms/km², and 2.87 ha/km² at altitudes
105 above 1540 meters) of rock glaciers in the Romanian Carpathians (Onaca et al., 2017b) (Fig. 1). The range also hosts the longest
106 Carpathian rock glacier, Valea Rea, extending 1.4 km (Urdea, 2000) (Fig. 2b). According to Necsoiu et al. (2016), slow-moving
107 rock glaciers in the Southern Carpathians increased their velocities by 20% between 2007 and 2014, likely due to rising
108 permafrost temperatures.

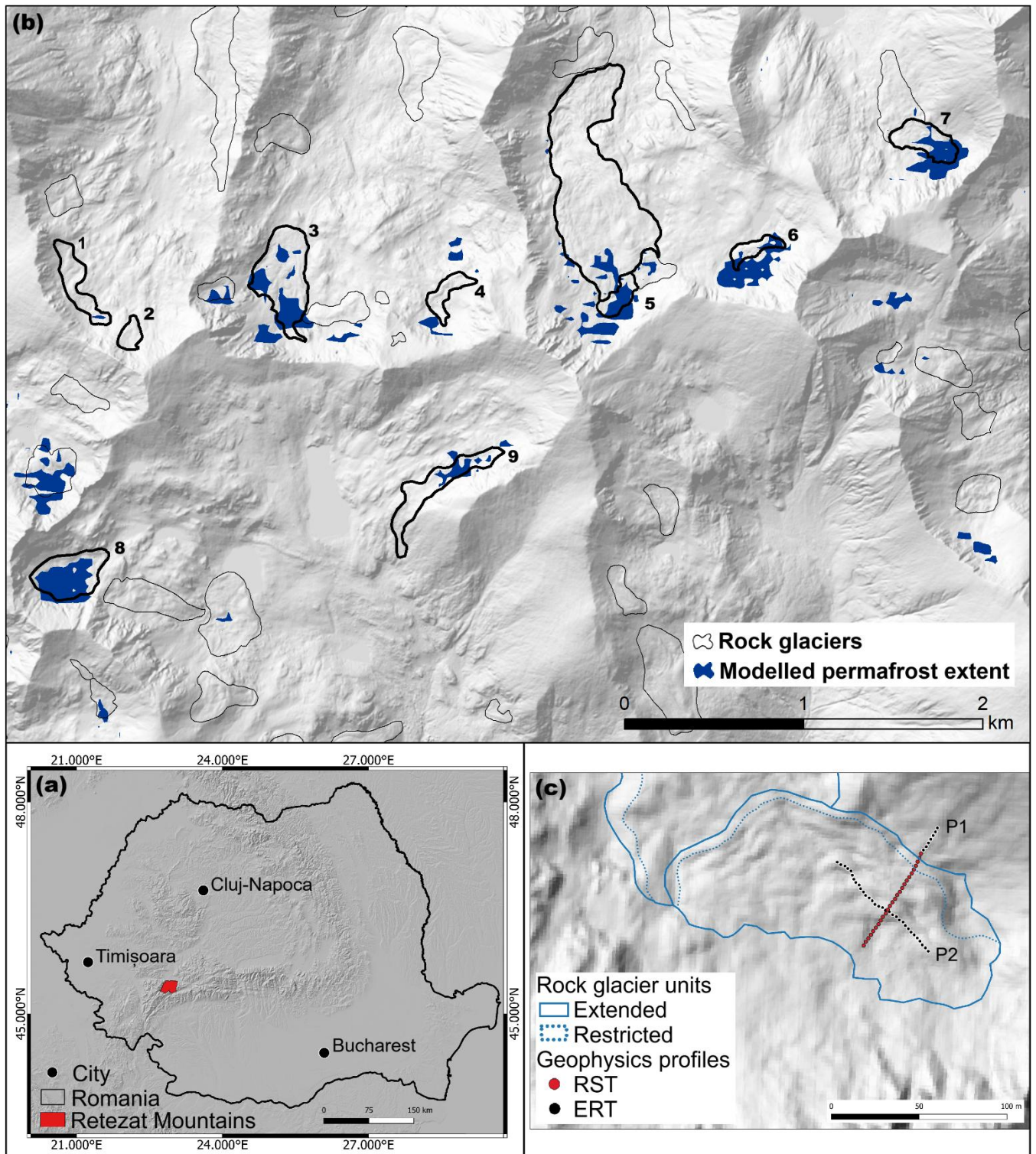
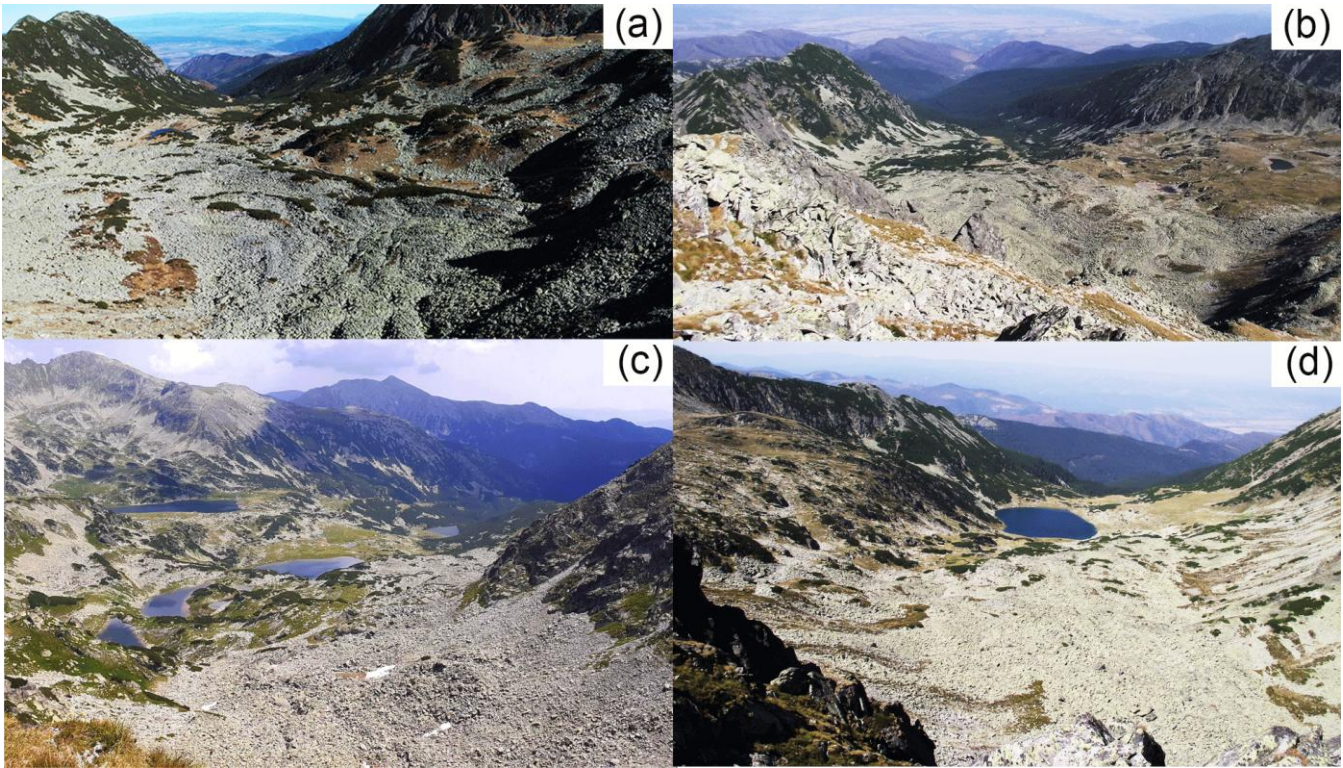


Figure 1: Study sites. (a) Overview map with the location of the Retezat Mountains in Romania, background of the map: hillshade based on FABDEM (Howker et al. 2022). (b) modelled permafrost extent (Popescu et al., 2024) and spatial distribution of rock glaciers in the Retezat Mountains overlaid on a hillshade based on the LAKI II DEM (LAKI II MNT, 2024). The rock glaciers that are discussed in the present paper are mapped with thicker lines and are presented in Table 1. (c) A detailed map with the position of the geophysics profiles on Galeşu rock glacier; note: same background image as (b).

121 **Table 1** Rock glaciers investigated through ground-based measurements and/or discussed in this study (BTS = bottom temperature
122 of snow cover; GST = ground surface temperatures ERT = electrical resistivity tomography; RST = refraction seismic tomography,
123 dGNSS = differential GNSS measurements).

Number in Fig.1	RG name	RG activity	Ground-based measurements type
1	Stânișoara	Relict	-
2	Bucura	Transitional	-
3	Pietrele	Relict	BTS, GST
4	Pietricelele	Transitional	BTS
5	Valea Rea	Relict	GST
6	Păpușa	Transitional	BTS
7	Galeșu	Transitional	BTS, GST, ERT, RST
8	Judele	Transitional	GST, dGNSS
9	Berbecilor	Transitional	dGNSS

124



125

126 **Figure 2: Pictures of rock glaciers from Retezat Mountains: a) Pietrele (3) – relict; b) Valea Rea (5) – transitional; c) Judele (8) –**
127 **transitional; d) Galeșu (7) – relict. Photo credit: A. Onaca.**

128 3. Methods

129 3.1. Rock glacier inventory

130 Rock glaciers are classified into three categories based on activity: active, transitional, and relict, (RGIK, 2023a). Active rock
131 glaciers exhibit consistent downslope movement across most of their surface, with displacement rates ranging from a decimetre
132 to several meters per year (RGIK, 2023a). Most of the surface of a transitional rock glacier experiences little to no downslope
133 movement, with annual average displacement rates generally falling below one decimetre (RGIK, 2023a). Rock glaciers
134 exhibiting no detectable movement across most of their surface are classified as relict (RGIK, 2023a).

135 This study updates the existing inventory of Southern Carpathians rock glaciers (Onaca et al., 2017b) following RGIK (2023a)
136 guidelines. The inventory involved mapping rock glaciers through fieldwork surveys and detailed examination of high-resolution
137 aerial imagery. Due to the limited kinematic data (Vespremeanu-Stroe et al., 2012; Necsoiu et al., 2016), the current inventory
138 lacks data on the activity of rock glaciers. Information on rock glacier kinematics was only available for a few landforms
139 (Vespremeanu-Stroe et al., 2012; Necsoiu et al., 2016), while most of the rock glaciers were classified as either intact or relict
140 based on geomorphological and ecological criteria (e.g., degree and type of vegetation cover).

141 **3.2. Persistent scatterer interferometry using Sentinel-1 data**

142 PSInSAR is a remote sensing technique designed to measure ground displacements along the radar line of sight (SAR LOS)
143 with millimetric accuracies (Rucci et al., 2012; Yu et al., 2020). Although Sentinel-1 (S1) SAR data does not offer the highest
144 spatial resolution, its global coverage, regular acquisition and open access policy have enabled large-scale ground motion
145 monitoring since 2014, resulting in a growing archive of applications.

146 Sentinel-1 serves as the backbone of the operational PSInSAR application under the European Ground Motion Service (EGMS),
147 which provides open-access ground motion data across Europe. The PSInSAR analysis in this study, developed by Terrasigna,
148 generally follows EGMS specifications (EEA, 2025), but differs in key areas, including reference point selection, atmospheric
149 modelling in steep terrain and SAR image selection. EGMS computes ground motion at the regional scale, using reference points
150 mainly in lowland areas where infrastructure ensures strong and stable radar backscatter. It also includes all available
151 acquisitions, even those affected by snow cover at high altitudes. However, inspection of EGMS products reveals that extending
152 the measurement network from lowland reference points to mountain summits has proven ineffective. This is mainly because
153 the atmospheric path delay associated with steep topography was not adequately compensated for and acts like phase noise.
154 Snow cover further degrades data quality by scattering radar signals and increasing phase noise, especially when snow is non-
155 uniform or has variable humidity. Under dry snow conditions, radar waves penetrate the snowpack, but because they propagate
156 more slowly than in air, the interferometric phase experiences a time delay, that appears as false subsidence (i.e., ground
157 displacement away from the radar sensor). These factors often result in the rejection of radar targets on mountain tops due to
158 excessive noise.

159 To address these challenges, Terrasigna carefully selected reference points on mountain summits, where the topographic
160 atmospheric delay is similar to that of the areas of interest. Additional efforts were made to improve the accuracy of atmospheric
161 delay modelling and compensation and limited analysis to snow-free acquisitions. Consequently, a high density of radar targets
162 on bare rock surfaces at mountain tops was preserved in our measurements.

163 Both ascending and descending paths were processed for cross-validation, along with L-band ALOS data. Because descending
164 passes occur in the early morning – when atmospheric conditions are generally more stable than in the evening – the resulting
165 measurements tend to be less noisy. A 2D decomposition between ascending and descending passes is technically feasible;
166 however, the steep topography introduces several challenges. First, areas that are clearly visible from one orbit may be in shadow
167 or appear foreshortened in the other, reducing data quality and spatial consistency. Second, since the topography is steep, the
168 preferential direction of ground movement is often dictated by the slope of the terrain. Additionally, the 2D decomposition
169 estimates vertical and east-west displacement components under the assumption that there is no north-south movement – an
170 assumption that is frequently invalid in mountainous regions, where north-south displacement is commonly observed. Given
171 these challenges, only the orbit with the best results was used for validation and mapping.

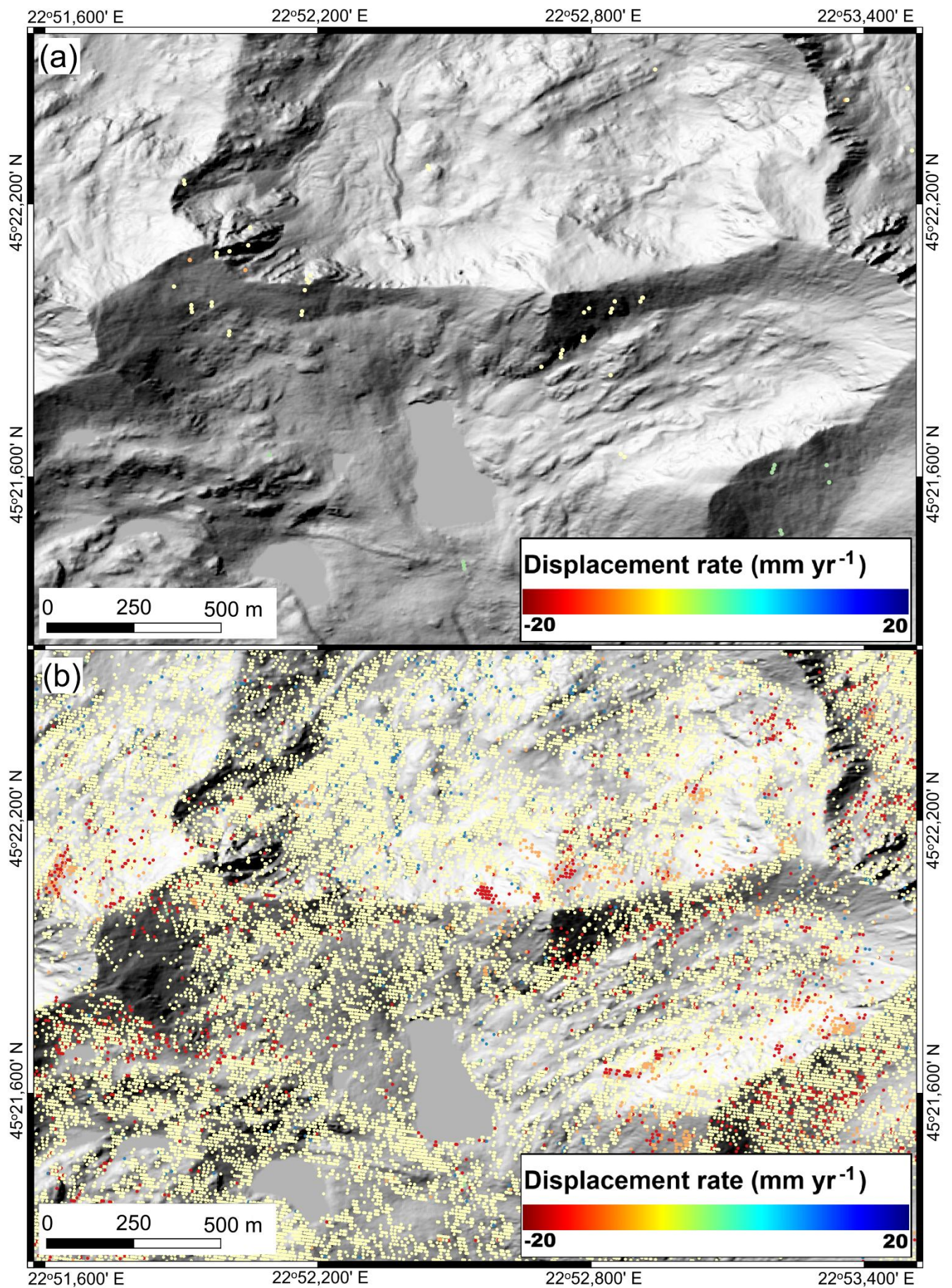


Figure 3: Comparison between the PSInSAR spatial density of measurements obtained by EGMS (a) and Terrasigna (b) in the central area of Retezat Mountains. Background of both maps: hillshade based on the LAKI II DEM (LAKI II MNT, 2024).

Figure 3a illustrates the total coverage from all S1 paths (Ascending and Descending orbits) in the study area using the EGMS product, while Figure 3b shows the PSInSAR analysis from a single S1 path (Path 80 Descending), hereafter called 'Terrasigna PSInSAR'. It is evident that the EGMS coverage is sparse and does not highlight dynamic areas – there are no zones marked in red, which typically indicate significant ground motion. In contrast, Terrasigna PSInSAR offers denser coverage and clearly highlights dynamic areas, with red colours denoting higher displacement rates.

This study assessed rock glaciers kinematics using 181 snow-free S1 images acquired between May 15, 2015, and October 4, 2021 to avoid coherence loss. Motion was measured along the SAR LOS direction; however, the actual displacement of the rock glacier surface is expected to mainly occur along the slope or in the vertical direction. The PSInSAR algorithm (Rucci et al., 2012; Crosetto et al., 2012; Poncoş et al., 2022), preserved all displacement information to maximize the chances of detecting slow movements (mm yr^{-1}) in unvegetated areas. The process began by extracting linear deformation information before applying any spatial or temporal filtering, which was typically used to improve phase statistics. A major challenge is that atmospheric phase is two orders of magnitude larger than the displacement signal (Poncoş et al., 2022), requiring meticulous phase unwrapping and correction of each residual interferogram. Notably, 24 out of 94 rock glaciers in the area are oriented north-south or south-north, potentially causing underestimation of along-slope displacements due to limited satellite sensitivity to slope-parallel motion.

The PSInSAR results were analysed using the Persistent Scatterers Online Software Tool (PSTool), a web-based platform developed by Terrasigna Inc. (Poncoş et al., 2022), designed to handle large volumes of ground displacement data. PSTool enables inspection of temporal ground motion characteristics, selection of areas of interest, extraction of temporal averages of displacement rates, export of temporal profiles in standard formats for integration with user platforms, and uploading of user-specific layers on top of the displacement information.

3.3. Inventorying moving areas

Following RGIK (2023a) guidelines, a moving area (MA) represents an area at the surface of the rock glacier characterised by homogeneous velocity rates and consistent flow direction. Based on multi-annual surface velocity from Terrasigna PSInSAR, MAs were identified within the inventoried rock glaciers (Onaca et al., 2017b) and classified into SAR velocity classes (Barboux et al., 2014; Bertone et al., 2022): $0.3\text{--}1\text{ cm yr}^{-1}$, $1\text{--}3\text{ cm yr}^{-1}$, and $3\text{--}10\text{ cm yr}^{-1}$, undefined (RGIK, 2023a) (Fig. 4). The velocity class characterizes the average yearly displacement rate recorded within a MA during the 2015–2021 period. The undefined class was assigned to MAs characterised by inhomogeneous velocity rates. Displacements $\leq 0.3\text{ cm yr}^{-1}$ were assigned to the “no movement” category, as this threshold was considered the lower limit of velocity detection on S1 interferograms in this type of approach (Rouyet et al., 2021). The moving areas were manually digitized and compiled into an inventory using ArcGIS 10.8. MAs smaller than 1000 m^2 were excluded to avoid signals from active layer deformation unrelated to permafrost creep. Spatial analysis used a one-meter resolution digital elevation model derived from 2018 high-resolution LiDAR data (LAKI II MNT, 2024).

3.4. Differential GNSS measurements

Judele (8) and Berbecilor (9) rock glaciers were surveyed by differential GNSS (DGNSS) measurements every summer between 2019 and 2021. A differential dual-frequency Topcon Hiper V GPS had acquired high-precision positioning data in real-time kinematics mode. The dGNSS device uses two receivers, one installed as a fixed base station, whereas the roving receiver was moved in the field. The mobile receiver gets the corrected position information calculated by the base station via a radio signal in order to measure a point with very high precision (i.e. $< 1\text{ cm}$ accuracy in the horizontal plane). 25 survey markers were measured in October 2019 and remeasured in October 2020 and 2021. Additionally, two control points on stable bedrock outside the rock glaciers boundaries, were measured to assess DGNSS horizontal accuracy, which ranged from 0.3 to 0.6 mm/yr^{-1} . Velocities were calculated as the displacement between the initial and final positions over the two-year period.

217 3.5. Validation with ALOS-2 PALSAR-2 interferometry

218 To validate Terrasigna's PSInSAR analysis developed for this study, six ALOS-2 PALSAR-2 images acquired between 2014
219 and 2019 during snow-free periods (September -October) were analysed. Wrapped differential interferograms were computed
220 for time intervals of one to five years using a 10 m resolution DEM derived from 1:25 000 topographic maps with 10 m contour
221 lines. Areas affected by geometric distortions were masked and only reliable signals from descending paths were used.. Moving
222 areas were independently identified and delineated, and then associated to the existing Rock Glacier Units (RGUs) (RGIK,
223 2023b).

224 3.6. Thermal conditions

225 The bottom temperature of the winter snow cover is an efficient method to map permafrost distribution in non-arid mountains
226 (Vonder Mühl et al., 2002). Under optimal snow conditions, BTS values indicate probable permafrost at < -3 °C, possible
227 permafrost at -2 to -3 °C and absence of permafrost at > -2 °C (Haeberli, 1973; Hoelzle, 1992; Popescu et al., 2024). However,
228 on dry, porous bouldery surfaces - where air convection and advection occur - BTS loses accuracy in precisely identifying
229 permafrost (Bernhard et al., 1998). Still, it remains highly effective for distinguishing colder ground from warmer ones. In March
230 2022, 140 BTS measurements were recorded using two classical 2.6 m-long probes with digital thermometers (± 0.5 °C
231 accuracy).. Measurements were taken at the snow-ground interface on four rock glaciers across three north-facing valleys in the
232 central Retezat Mountains (Fig. 1). Snow depths at all sites exceeded 80 cm, ensuring insulation from air temperature
233 fluctuations (Ishikawa et al., 2003). Previous studies in the Southern Carpathians (Vespremeanu-Stroe et al., 2012; Onaca et al.,
234 2015) confirm that BTS values remain stable in March beneath thick snow that typically accumulates in November or December.
235 Miniature temperature data loggers became widely used in mountain permafrost terrain to better understand surface energy
236 exchange fluxes (Hoelzle et al., 1999). Four rock glaciers in the central part of the Retezat Mountains were instrumented to
237 monitor the thermal regime at the ground surface (Fig. 1b). GST was recorded every 2 hours using iButtons DS1922L data
238 loggers, which operate between -40 and 80 °C with a manufacturer-stated accuracy of ± 0.5 °C. The sensors were indirectly
239 calibrated at 0 °C using the snow melting period ("zero curtain" interval). In mid to late winter, ground surface temperatures
240 tend to stabilize beneath thick snow, with subsurface processes controlling energy exchange. This stable phase, known as the
241 "winter equilibrium temperature" (WEqT) is a reliable empirical indicator of permafrost existence when values are below -2 °C
242 (Sattler et al., 2016). WEqT typically lasts at least two weeks and occurs under snow cover thicker than 50 cm (Schoeneich,
243 2011). Both WEqT and mean annual ground surface temperature (MAGST) were calculated for each GST monitoring site.

244 3.7. Geophysical Methods and PJI Modelling

245 Geophysical methods, such as electrical resistivity tomography and refraction seismic tomography, are widely applied in
246 mountain permafrost studies to characterise subsurface structure and heterogeneity and to detect and map ground ice occurrences
247 (Hauck et al., 2011; Herring et al., 2023). Both methods are sensitive to differences between frozen and unfrozen subsurface
248 conditions. Since ice acts as an electrical insulator as opposed to water, the electrical resistivity increases exponentially with
249 decreasing temperatures below 0 °C. Similarly, the seismic P-wave velocity of ice is with 3500 m s⁻¹ higher than that of liquid
250 water (~ 1500 m s⁻¹) or air (330 m s⁻¹), allowing frozen sediments (containing ice) to be distinguished from unfrozen ones (pore
251 space filled with water or air).

252 ERT is the most common geophysical technique applied in permafrost research and is used for mapping permafrost occurrence
253 where no borehole information is available, as well as monitoring changes in the ice-to-water ratio (Wagner et al., 2019; Mollaret
254 et al., 2020). The RST method is often used as a complementary method to ERT to reduce the ambiguity in the interpretation of
255 ERT data, as the P-wave velocity (v_p) is mainly controlled by density. Variations in v_p allow to identify porosity changes, or to
256 discriminate between liquid (water) and solid (ice) pore fluid, as well as in determining the depth to the bedrock.

257 In the absence of ground truth information about the state of permafrost, another advantage of geophysical data is, that co-
 258 located ERT and RST data can be used to quantitatively estimate the content of the four phases (i.e., rock, ice, water and air)
 259 using the so-called 4-phase model approach, which relies on the petrophysical equations by Archie (1942) for the electrical
 260 resistivity and that of Timur (1968) for the P-wave velocity.

261 Recently, the approach has been further developed by Wagner et al. (2019), to the so-called petrophysical joint inversion (PJI)
 262 framework, permitting the joint inversion of ERT and RST data sets to simultaneously solve for the subsurface distribution of
 263 the 4 phases. The main advantage of the PJI lies in its improved accuracy, as it iteratively seeks a subsurface model that fits both
 264 seismic and resistivity data. This leads to a more realistic representation of porosity compared to earlier versions of the 4-phase
 265 model (Hauck et al., 2011). Mollaret et al. (2020) demonstrated the applicability of the PJI for data collected on different alpine
 266 permafrost landforms with different ice contents.

267 In the field, 2D ERT data were collected using a GEOTOM (Geolog) multi-electrode system equipped with 50 electrodes spaced
 268 4 meters apart. By combining a multitude of individual measurements with different electrode combinations (i.e. quadrupoles)
 269 along a profile line, a 2-dimensional resistivity model of the subsurface is obtained. All surveys employed the Wenner
 270 configuration, which provides an optimal signal-to-noise ratio, which is especially important in dry and coarse-blocky terrain.

271 2-dimensional RST data were obtained using a 24-channel Geode seismometer (Geometrics). An artificial seismic wave is
 272 produced by hitting a sledgehammer to the ground, and the waves travel along different paths through the subsurface and back
 273 to the surface, where they are registered by 24 geophones. The subsurface structure and composition can be derived from the
 274 travel time the so-called P-wave needs from the source (i.e. hammer) to the geophones. The wave velocity (v_p in $m\ s^{-1}$), and
 275 thus the travel time, is basically a function of the density of the subsurface material, and the obtained seismic velocity allows
 276 inferring the subsurface material. The pre-processing of the seismic field data (picking of first arrivals) was performed using the
 277 software ReflexW (Sandmeier, 2020). The individual ERT and RST data sets were initially inverted independently using the
 278 PyGimLi framework (Rücker et al., 2017), followed by a petrophysical joint inversion to estimate ground ice contents using the
 279 approach developed by Wagner et al. (2019).

280 **4. Results**

281 **4.1. Inventorying moving areas**

282 In the Retezat Mountains the MAs exhibited velocities ranging from 0.3 to 5 $cm\ yr^{-1}$ (Fig. 4 and 5). The measured displacement
 283 between 2015 and 2021 remained constant for most MAs, with no significant temporal variations (see trendlines in Fig. 5).
 284 Given the relatively low velocities of the MAs, seasonal variations were difficult to assess reliably; thus, only annual or
 285 multiannual rates were considered.

286 A total of 92 MAs covering 0.27 km^2 were inventoried within the Retezat Mountains rock glaciers. Most MAs fall into the slow
 287 velocity classes of 0.3 – 1 $cm\ yr^{-1}$ and 1-3 $cm\ yr^{-1}$ (Fig. 6), with only 10 % exhibiting velocities of 3-10 $cm\ yr^{-1}$ (Fig. 6a). About
 288 37 % of the rock glaciers contain MAs, which typically occupy less than 30 % of each rock glacier's surface; however, in six
 289 cases, the cumulated area of MAs represents more than 50 % of the rock glacier area (Fig. 6d). The mean MA area is 0.3 ha,
 290 ranging from 0.1 to 1.77 ha.

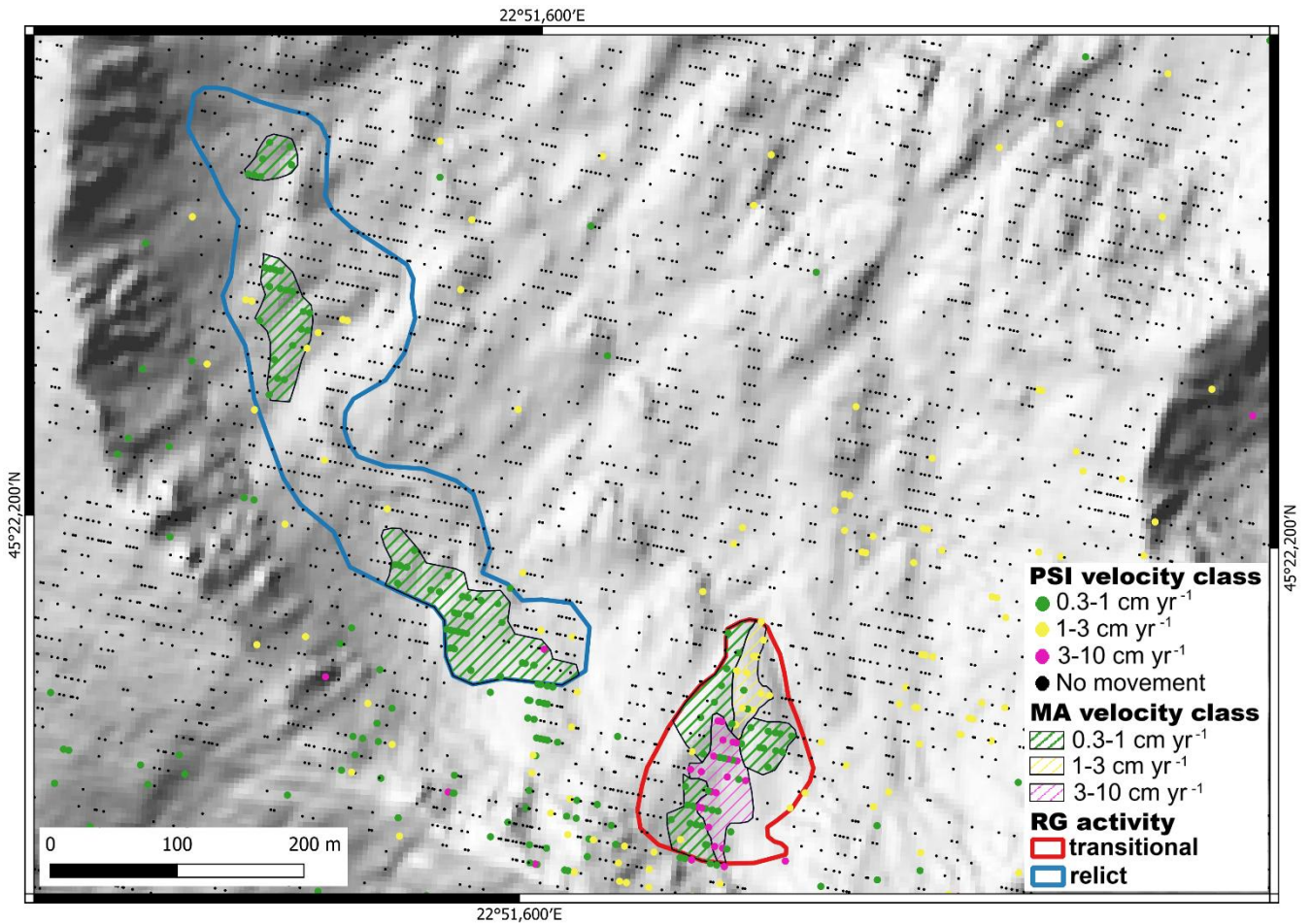


Figure 4: Example of moving areas and rock glacier activity for the Retezat Mountains. The two RGs are marked with numbers 1 and 2 in fig.1. Background image: hillshade based on the LAKI II DEM (LAKI II MNT, 2024).

The number of MAs per rock glacier ranges from 1 and 8, with the majority (69 %) containing 1 to 3 MAs. MAs with velocities $> 3 \text{ cm yr}^{-1}$ were identified in 8 rock glaciers, while those in the $1\text{--}3 \text{ cm yr}^{-1}$ class were found in 17 (Fig. 6c). The median elevation of MAs by velocity class ranges from 1950 and 2295 m (Fig. 7). Most MAs (62 %) are located between 2100 and 2200 m, followed by 17 % between 2200 and 2295 m, 16 % between 2000 and 2100 m, and only 5 % are below 2000 m. Higher velocity classes ($1\text{--}3$ and $3\text{--}10 \text{ cm yr}^{-1}$) tend to occur at the highest elevations (Fig. 7a Slope values across MAs vary between 8° and 42° , with the widest range observed in the $0.3\text{--}1 \text{ cm yr}^{-1}$ class, which also shows higher median slopes (Fig. 7b). Half of the MAs (50 %) face north (Fig. 8), despite that only 21 % of the inventoried rock glaciers in the Retezat Mountains stand out on the northern aspects. NE and E slopes host 32 % of MAs compared to 23% on NW and W aspects, relative to rock glacier distribution (Fig. 8). Across the mountain range, western aspects dominate in surface area. MAs with velocities $> 3 \text{ cm yr}^{-1}$ receive the lowest potential solar radiation (Fig. 7c).

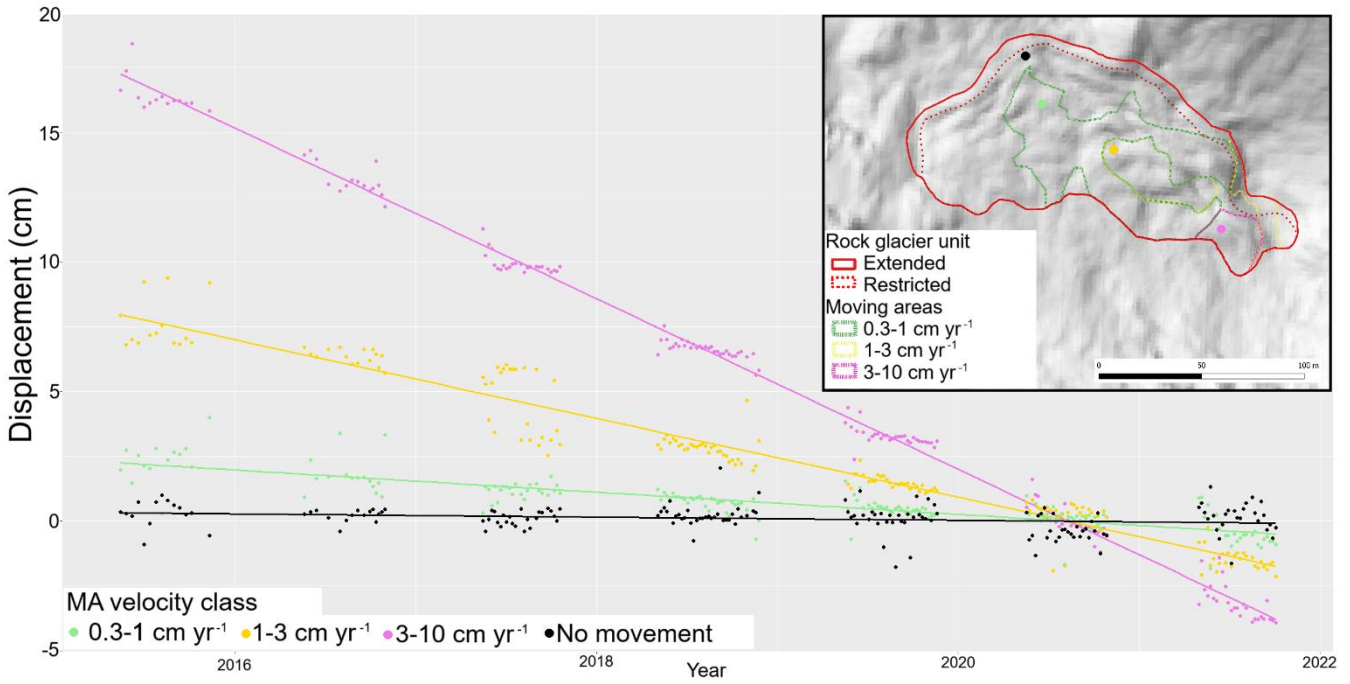


Figure 5: Displacement profiles over a period of 6 years (2015 – 2021) for 4 locations (identified in the location map with dots of corresponding colour) representing each velocity class and one for an area with no movement. The dots show the actual PSI displacement results, while trend lines (linear regressions) indicate long-term motion patterns. The displacement is measured relative to 2021. The downward trend can be interpreted as movement away from the sensor, which in our case represents a combination of vertical movement and horizontal downslope movement. The gap in point density along the trend line is due to the winter season, the measurements being performed in snow free conditions, usually from June to November.

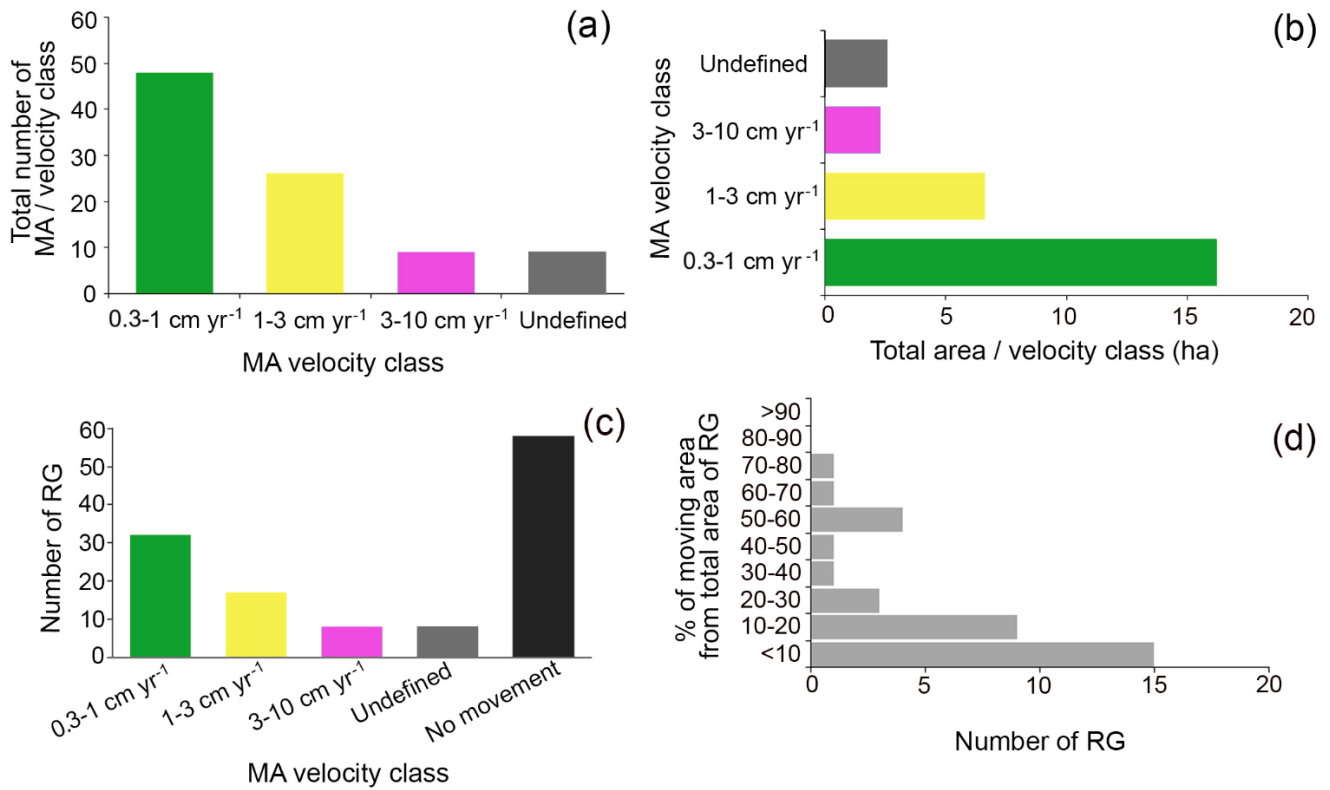


Figure 6: The moving areas classified by velocity classes (a) and their extent (b). The number of rock glaciers containing moving areas and without moving areas (c) and the percentage of the moving area cover within rock glaciers (d).

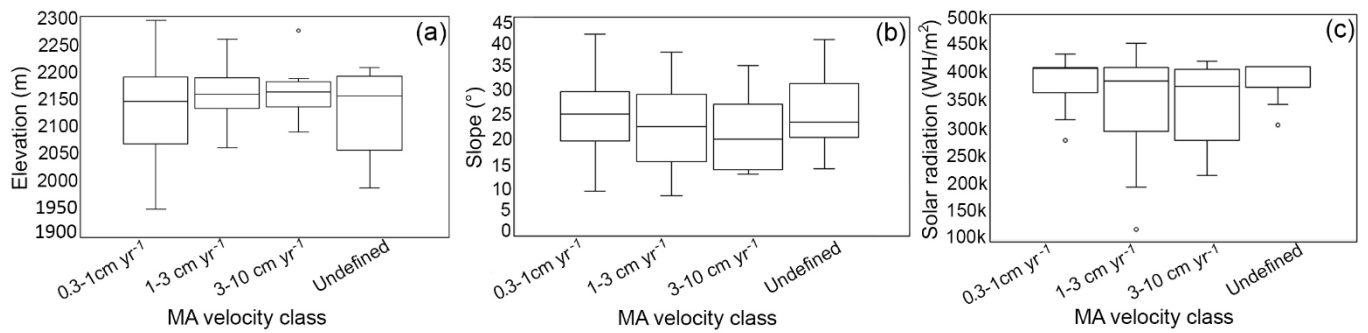


Figure 7 Elevation (a), Slope (b) Potential solar radiation (c) vs MA velocity classes

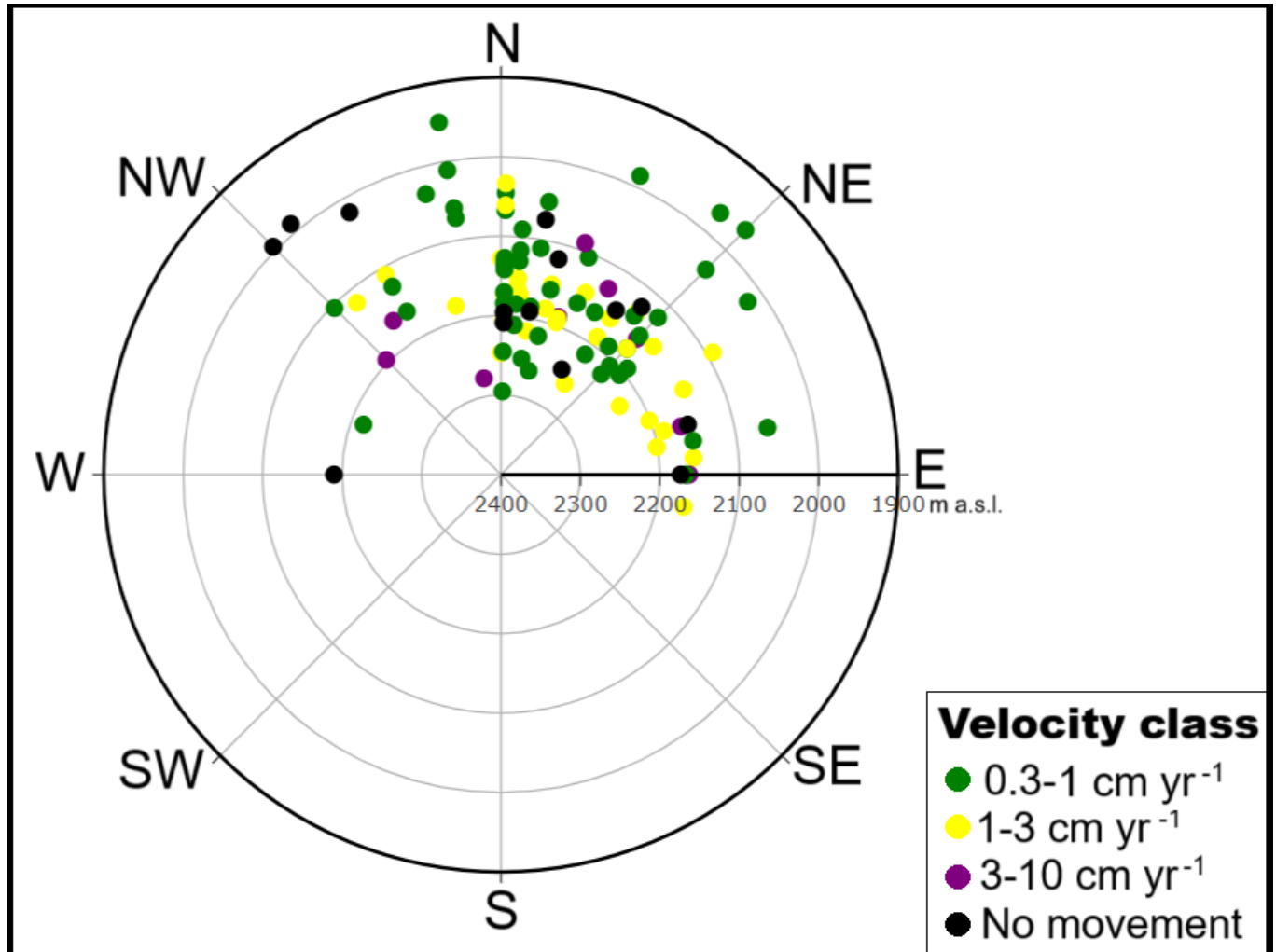


Figure 8: Distribution of moving areas, in the Retezat Mountains, in relation to slope aspect (angular axis) and elevation (radial axis).

For rock glaciers exhibiting no or minimal movement ($< 1 \text{ cm yr}^{-1}$), the RGIK (2023a), recommends assigning a relict activity class. Based on this criterion, only 21 % of the rock glaciers in the Retezat Mountains are classified as transitional (Fig. 9a), with velocities between 1 and 5 cm yr⁻¹. Transitional rock glaciers have a higher median elevation (2170 m), about 150 m above the relict ones (Fig. 9b) and a slightly smaller median size (Fig. 9c).

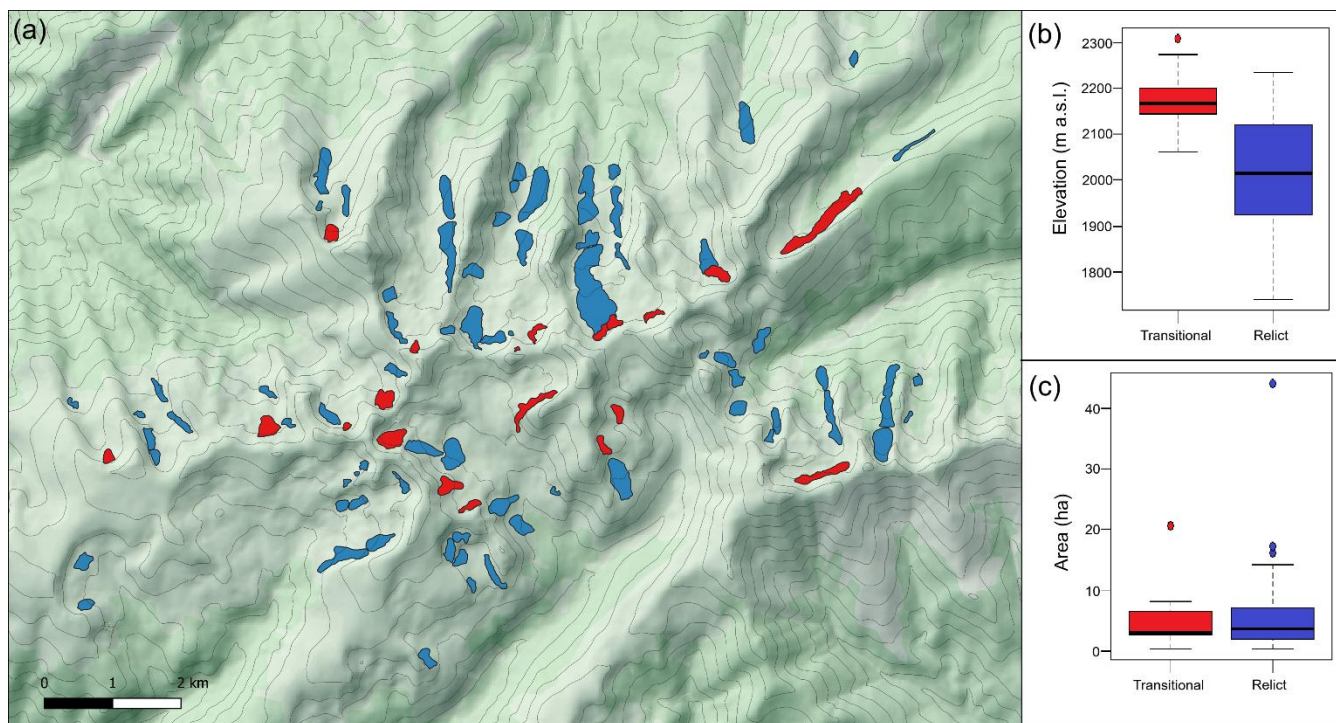


Figure 9: The spatial distribution of transitional and relict rock glaciers in the Retezat Mountains (a) and their median elevation (b) and size (c). Background imagery: Bing Maps © Microsoft, retrieved via QGIS (Version 3.34) using the QuickMapServices.

Figure 10 compares ALOS-2 PALSAR-2 interferogram with Sentinel-1 PSInSAR results at Galeşu (7) site. While the ALOS-2 PALSAR-2 has lower spatial resolution and accuracy, both datasets show consistent displacement signals, with main MAs clearly visible and overlapping. The comparison highlights that PSI provides finer spatial detail, particularly in areas with high displacement variability. In Fig. 10b, a specific MA is distinctly mapped with velocities $<1 \text{ cm yr}^{-1}$. The same zone in Fig. 10a shows a similar core of low velocity, but includes adjacent areas classified as $1\text{--}3 \text{ cm yr}^{-1}$ and $3\text{--}10 \text{ cm yr}^{-1}$, suggesting a broader range of motion detected by ALOS-2 PALSAR-2 interferogram.

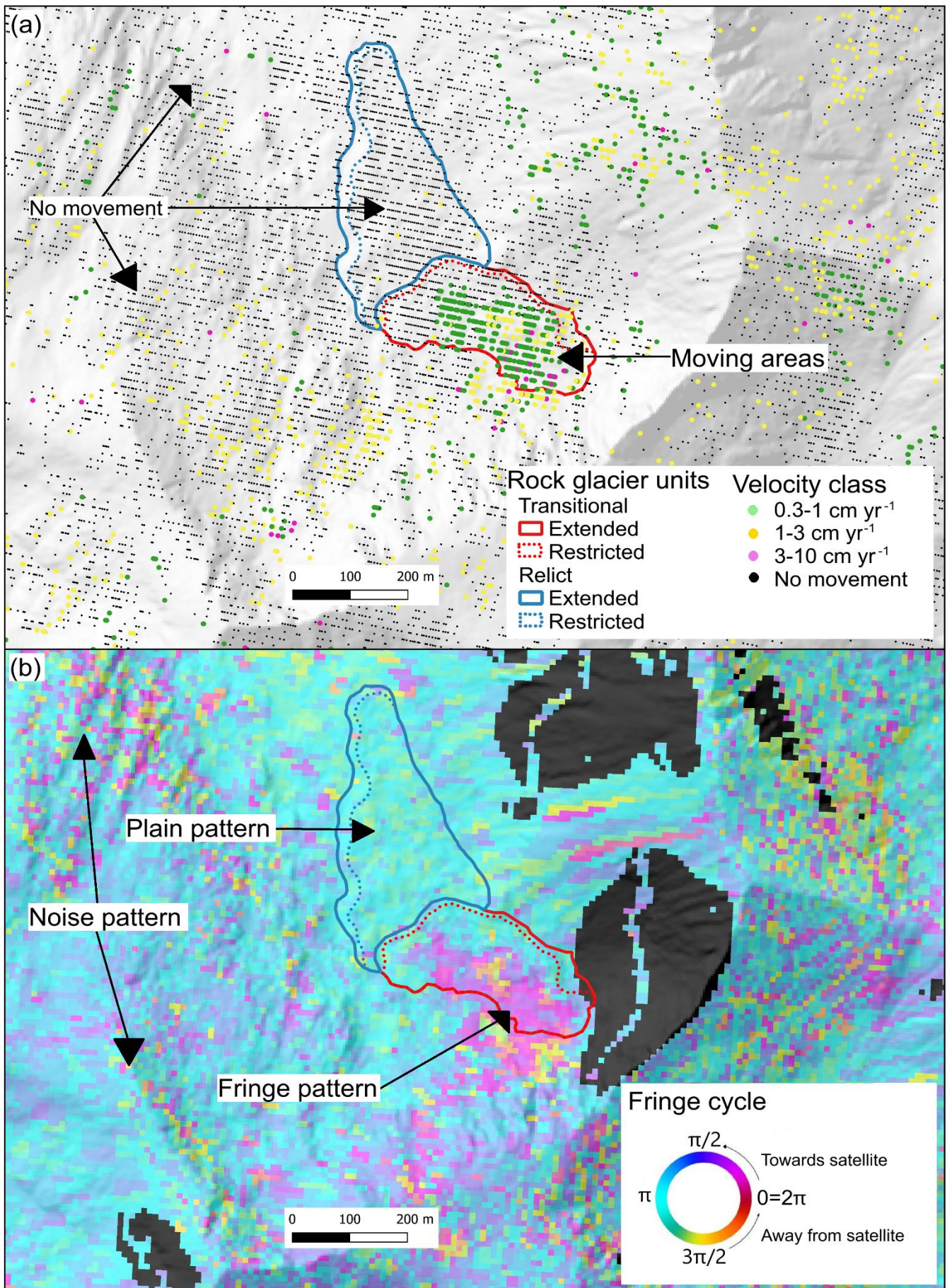
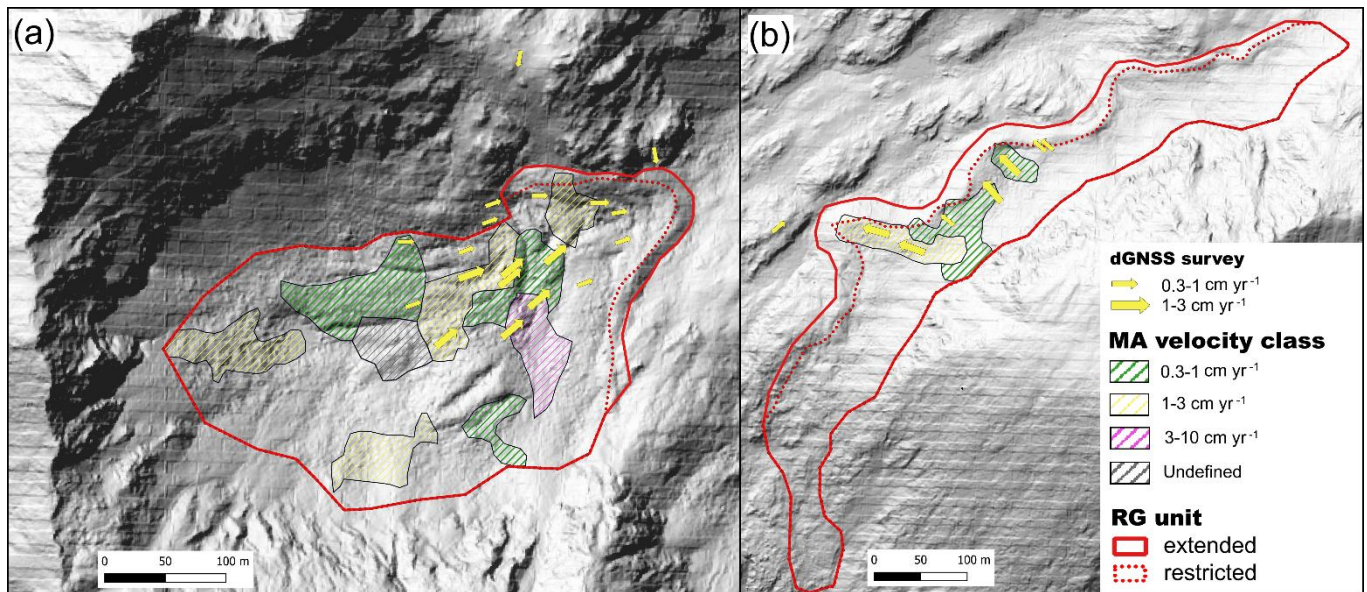


Figure 10: A comparison between multiannual PSINSAR from Sentinel 1 (a) and InSAR from ALOS-2 PALSAR-2 (b). Notice the same moving areas inside the RGs, that are revealed by clustered pixels with movement (green, yellow and magenta) from PINSAR (a) and the areas with fringe patterns (b). In (b) the shadow areas are masked out and the fringe cycle (bottom right) represents the change of colour. The interferogram presented in fig. 10b, over the Galeşu rock glacier unit, has a long temporal interval, over five years from September 2014 to October 2019, and it is computed only for the descending path.

344 4.2. GNSS measurements

345 The mean velocities measured by dGNSS ranged between 0.4 and 2.8 cm yr⁻¹, with values exceeding 1 cm yr⁻¹ for 56 % of the
 346 marker points (Fig. 11). On the Judele (8) rock glacier, eight marker points recorded velocities between 1 and 2.6 cm yr⁻¹, while
 347 nine points showed velocities between 0.4 and 1 cm yr⁻¹. The highest velocities are observed in the central part, gradually
 348 decreasing toward the margins. One marker point measured on the front of Judele rock glacier revealed very low rates of
 349 displacements (0.4 cm yr⁻¹). Almost all marker points indicate consistent movement toward the front of the rock glacier. Four
 350 marker points on the Berbecilor (9) rock glacier revealed velocities between 1 and 2.8 cm yr⁻¹ and three between 0.6 and 1 cm
 351 yr⁻¹. All the seven marker points indicate consistent movement toward the front. Most marker points with moving velocities
 352 between 1 and 2.8 cm yr⁻¹ (89 %) were located within MAs categorised under the 1-3 and 3-10 cm yr⁻¹ velocity classes by
 353 PSInSAR analysis. At Judele, five out of eight dGNSS markers recording velocities between 1 and 2.6 cm yr⁻¹, fall within the
 354 1-3 cm yr⁻¹ velocity class, whereas at Berbecilor the ratio is two out of four. At both sites, nine marker points with velocities
 355 between 0.4 and 1 cm yr⁻¹ are located outside any designated MAs, while only three fall within the corresponding velocity class.
 356

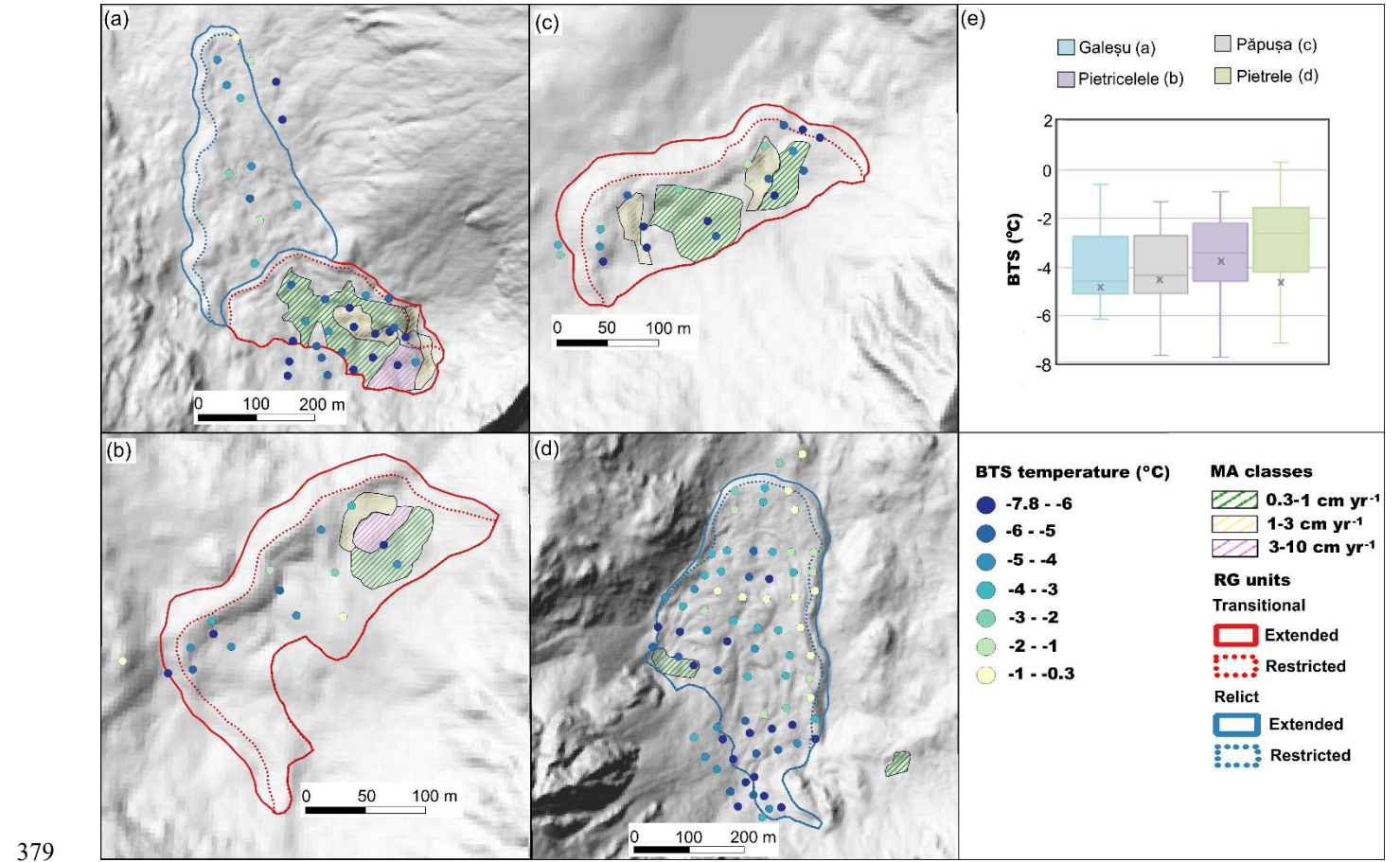


357
 358 **Figure 11: Horizontal displacements derived from GNSS measurements for 2019-2021 at Judele (a) and Berbecilor (b) sites, overlaid**
 359 **on the MAs derived from PSInSAR. Background of both maps: hillshade based on the LAKE II DEM (LAKE II MNT, 2024)**

361 4.3. BTS and ground temperatures

362 BTS measurements identified colder and warmer ground surface areas across four rock glaciers (Fig. 12). Half of the 140 BTS
 363 points were collected on Pietrele (3), the lowest-elevation site, which showed the warmest average BTS value (-2.9 °C). The
 364 coldest values occurred in its upper section (mostly < -3 °C), with several low readings also on the feeding talus slope. In the
 365 western part, where a 0.3-1 cm yr⁻¹ MA is present, BTS values were consistently below -5 °C. Galeşu, a multi-unit rock glacier,
 366 had a mean BTS of -3.9 °C, with the coldest values clustered in the southern unit and on the upslope talus. The BTS values
 367 within the MAs were all very low, below -5 °C. In contrast, the northern rock glacier unit, which showed no signs of surface
 368 displacement, exhibited a highly heterogeneous distribution of BTS values. Păpuşa (6), the highest site, recorded the lowest
 369 average of BTS values (-4.1 °C), while Pietricelele (4), had a mean of -3.5 °C. At Păpuşa, a small central zone had warmer BTS
 370 values (> -2 °C), but all MAs showed very cold conditions. Similarly, at Pietricelele, warmer areas were found in the central
 371 and northeastern parts, while the western and southeastern areas revealed colder temperatures. Snow depth at the probing points
 372 ranged from 80 to 260 cm. At all sites, the median BTS in MAs was lower than the overall site median.

373 Between 2013 and 2022, MAGST values at the monitoring sites generally remained below 0 °C, ranging from -2.3 °C to +0.8 °C,
 374 with the coldest values at Galeşu and the warmest at Pietrele. Figure 13a illustrate the long-term evolution of GST using a
 375 running annual mean. Persistent subzero MAGST values were recorded only at Valea Rea (5) in all the years, while Galeşu
 376 showed below 0 °C values in all years except 2016. All sites recorded negative mean temperatures over the full monitoring
 377 period.
 378



379 **Figure 12: BTS measurements performed in March 2022 on four rock glaciers in the Retezat Mountains: (a) Galeşu, (b) Pietricelele,**
 380 **(c) Păpuşa, (d) Pietrele. (e) Summary box-plot diagram of the BTS measurements, the horizontal line drawn inside denotes the median**
 381 **BTS for each rock glacier, while the x represents the median BTS of the moving areas of each rock glacier). (f) the legend for the maps**
 382 **in (a), (b), (c) and (d).**
 383

384
 385 Fig. 13c reveals the mean daily temperature at the GST monitoring sites. The lowest GST values (< -10 °C) occurred between
 386 October-December under snow-free or thin snow cover conditions. This is because the insulating snow cover typically occurs
 387 in November/December, whereas the snow disappears in May or June. Although snow depths are generally sufficient to insulate
 388 the ground by January, notable ground cooling still occurred between January and March at all sites. At Galeşu, nearly every
 389 winter displayed short-term GST fluctuations indicating episodic ground-air thermal exchange. Similar, though less pronounced,
 390 patterns were also observed at Judele (e.g., winters 2013-2014 and 2017-2018), Pietrele (e.g., 2012-2013, 2013-2014, 2014-
 391 2015, 2016-2017 and 2021-2022) and Valea Rea (e.g., 2015-2016 and 2019-2020). In a few instances, inverse thermal
 392 relationships between ground surface temperature and air temperature confirmed internal ventilation through the coarse debris
 393 during winter. These thermal anomalies, likely driven by advective heat fluxes beneath thick snow contribute to the low MAGST
 394 observed in the rock glaciers. By March, GST typically stabilised, reflecting conductive heat transfer. In nearly all cases, the
 395 resulting WEqT were below -2 °C, indicating possible or probable permafrost occurrence (Fig. 13b). WEqT values higher than
 396 -2 °C were recorded only at Pietrele in late winters 2013 and 2014. At Valea Rea and Judele, most WEqT values ranged from -
 397 2 to -3 °C, while Galeşu, consistently showed significantly lower values.
 398

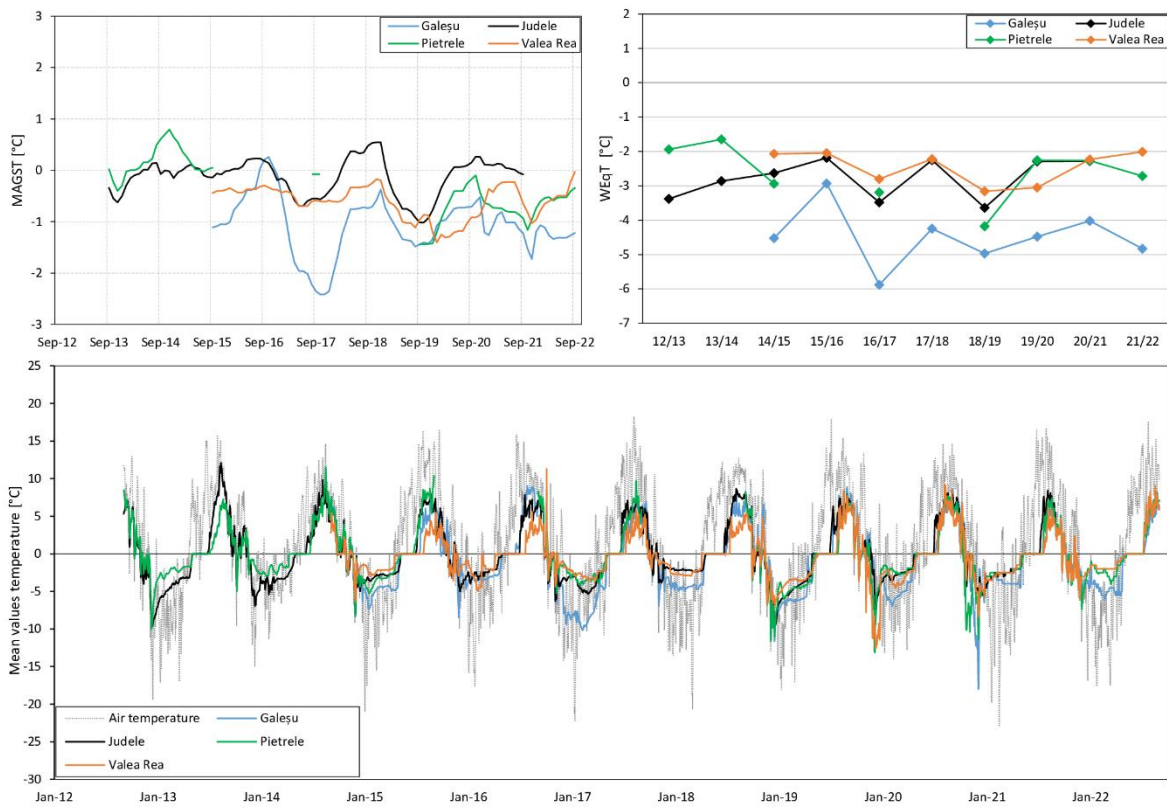


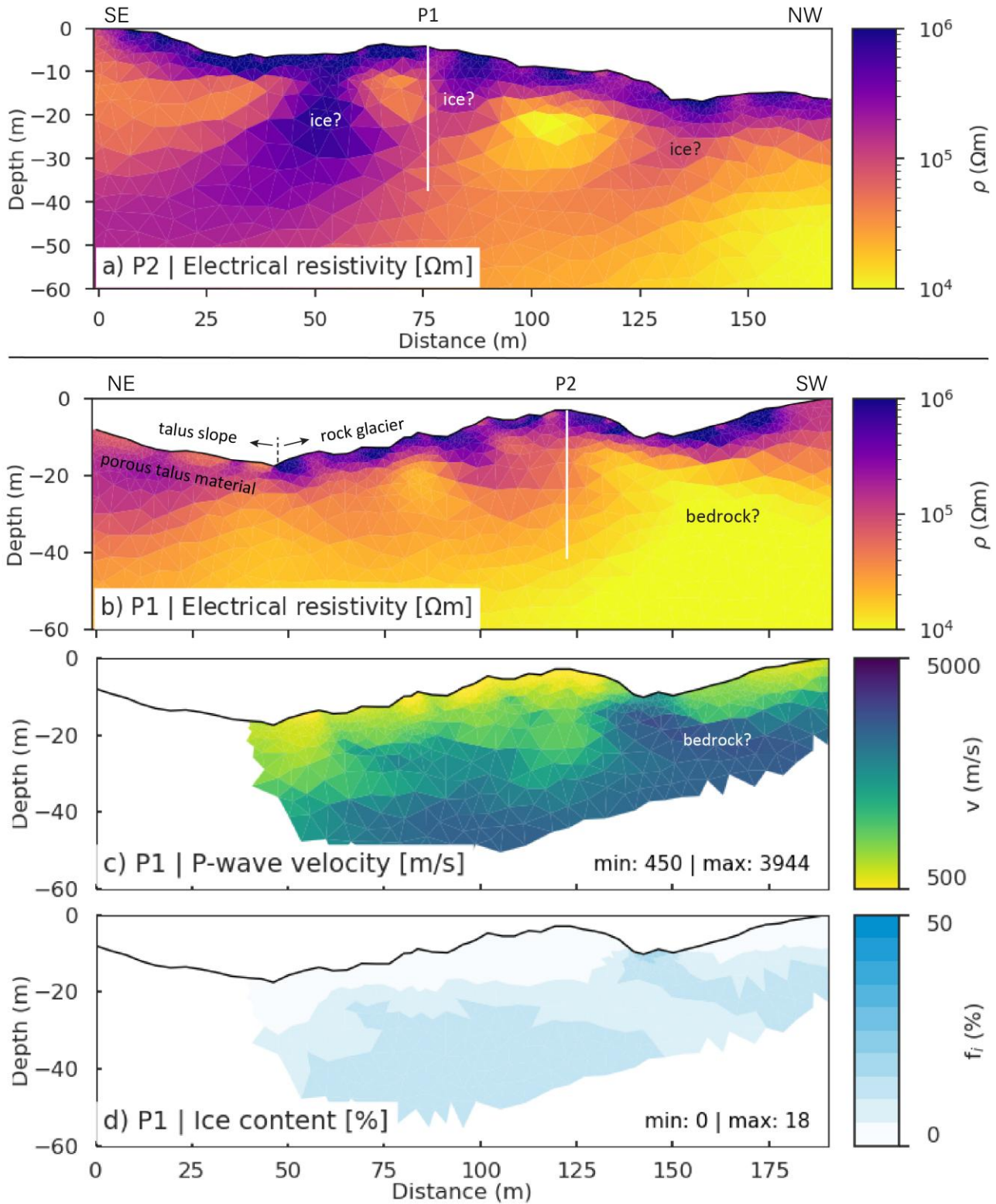
Figure 13: (a) Running 12-month average of mean annual ground surface temperature, (b) Winter Equilibrium Temperature (WEqT) and (c) Running 12 months average of Ground Surface Temperature (GST) for the period 2012/2013 to 2021/2022 at four sites in the Retezat Mountains and air temperature at Țarcu meteorological station (2180 m).

4.4. Geophysics results

The results of the geophysical surveys at Galeşu rock glacier are shown in Figure 14, including two crossing ERT profiles (P1 and P2) (Fig. 14a, b), as well as RST and PJI results available for profile P1 (Fig. 14c, d). Both ERT tomograms reveal an up to 5 m thick layer characterised by high resistivities ($> 200 \text{ k}\Omega\text{m}$) corresponding to the dry and coarse-blocky surface layer. Patchy occurrences with similarly high resistivities are observed in 5–20 m depth in both profiles, which could indicate remnants of former ice-rich permafrost within the rock glacier (labelled with 'ice?' in Fig. 14). Beneath these zones, a more homogeneous layer with resistivities around $10 - 30 \text{ k}\Omega\text{m}$ may indicate the rock glacier base (bedrock) in the southwestern part of profile P1, however, the resistivity values do not exclude the possibility of frozen conditions and the interpretations of this zone remains ambiguous. The landform's overall thickness is estimated at $< 20 - 30 \text{ m}$ and potentially $< 15 \text{ m}$ in the southwestern part of profile P1. The eastern part of profile P1 ($x < 50 \text{ m}$ in Fig. 14b) extends beyond the rock glacier into a partially vegetated talus slope. Here, the surface layer exhibits lower resistivities ($< 100 \text{ k}\Omega\text{m}$, probably representing smaller block size and organic material), and the underlying resistive layer ($100\text{--}200 \text{ k}\Omega\text{m}$) has a thickness of about 10 m and a more homogeneous appearance than that of the rock glacier. Both the morphology and the resistivity values point to a potentially frozen ventilated talus slope, but this is not a focus of this study and will not further be explored.

The seismic profile P1 (Fig. 14c) which covers only the rock glacier section of the ERT profile P1, reveals a 5–10 m thick upper layer with P-wave velocities $< 1500 \text{ m s}^{-1}$, indicating highly porous blocky material. The velocities are increasing with depth, reaching 4000 m s^{-1} at about 20–25 m depth in the central part of the rock glacier and at shallower depths ($\sim 15 \text{ m}$) toward the end of the profile. According to the seismic data, ice-rich permafrost would be possible in large parts of the tomogram. However, when combined with the ERT data, ice-rich conditions appear plausible in those parts of the tomogram that coincide with elevated resistivities. In contrast, areas with lower resistivities may reflect increased conductivity associated with ongoing ice

424 melt, rendering their interpretation ambiguous. The seismic data further indicate relatively porous material rather than firm
 425 bedrock and point to an overall larger thickness of the rock glacier than indicated by the ERT profile.
 426



427
 428 **Figure 14: a) and b) ERT profiles P2 and P1 (see Fig. 1c for location), c) RST profile, and d) modelled ground ice content based on the**
 429 **PJI.**
 430

431 The result of the PJI modelling (Fig. 14d) indicates generally very low ground ice content in the upper sector of the Galeşu rock
 432 glacier, with maximum values reaching only 18 %. The highest ice contents coincide with zones with highest seismic velocity,
 433 partly contradicting the individual interpretation (bedrock). This can be due to the known rock-ice ambiguity of the current PJI

434 formulation, as the rock and ice content are only directly constrained through the petrophysical equation of the seismic velocity.
435 Consequently, accurate differentiation between rock and ice can be problematic in some cases (see Mollaret et al., 2020 for
436 details). The overall low ice contents modelled through the PJI supports the interpretation that a formerly massive ice core is no
437 longer detectable, pointing to an advanced stage of degradation of this rock glacier. However, these results do not exclude the
438 possibility of more confined ice-saturated or even supersaturated layers (as expected based on the analysis of InSAR data in
439 section). Due to the limited resolution capacity of the geophysical profiles with 4 m sensor spacing, thin ice-rich or ice-
440 supersaturated layers may not be resolvable as such, but - depending on their depth and extent - with strongly reduced spatial
441 gradients of the ice content (as well as resistivity or velocity contrast in the individual tomograms). Therefore, the relatively
442 homogeneous ice content distribution in the PJI model may reflect both the intrinsic rock-ice ambiguity of the inversion
443 approach, and its limited ability to resolve small-scale subsurface structures.

444 **5. Discussion**

445 **5.1. Assessing the velocity of rock glaciers in marginal periglacial environments**

446 In marginal periglacial regions rock glaciers exhibit a minimal rate of motion (mm yr^{-1} to cm yr^{-1}) (Necsoiu et al., 2016) and
447 evaluating their velocity can pose occasional challenges. Hence, the compilation of MAs inventory might be affected by
448 limitations associated with radar interferometry (Bertone et al., 2022).

449 PSInSAR provides one-dimensional measurements along the satellite line-of-sight (LOS). capturing only a single component
450 of motion. Given the steep topography of the study area, it can be assumed that the movement direction of the actual motion is
451 oriented along the mountain slope. Although PSInSAR does not produce the exact 3-D velocity vectors, it proved effective for
452 detecting surface motion and refining the rock glaciers inventory.

453 Slow-moving areas (i.e., $0.3\text{--}1\text{ cm yr}^{-1}$; $1\text{--}3\text{ cm yr}^{-1}$) are prevalent in this region, with only 10% of MAs exceeding 3 cm yr^{-1} .
454 These faster MAs typically occur at higher elevations and receive less solar radiation than slower ones. Overall, the median MA
455 size in the Retezat Mountains is slightly smaller than in other periglacial regions (Bertone et al., 2022). The largest median size
456 (0.33 ha) occurs in MAs moving $< 1\text{ cm yr}^{-1}$, while those in the $1\text{--}3$ and $3\text{--}10\text{ cm yr}^{-1}$ classes have a median size of 0.3 ha —
457 approximately one-third smaller than those in South Tyrol (Bertone et al., 2024).

458 Differential GNSS measurements revealed similarly slow movements at selected points, ranging from a few millimetres to 2.8
459 cm yr^{-1} . Comparison with PSInSAR results showed limited agreement, likely due to the challenge both methods face in detecting
460 such low velocities, as well as differences in the observation periods (2015–2021 for PSInSAR vs. 2019–2021 for dGNSS).
461 Still, most GNSS survey markers with horizontal displacements exceeding 1 cm yr^{-1} were located within the MAs. In terms of
462 flow direction, the majority of these markers indicated consistent movement toward the fronts of Judele and Berbecilor rock
463 glaciers, behaviour characteristic of permafrost creep.

464 The PSInSAR analysis enriches the existing rock glacier inventory with information about the activity status of rock glaciers in
465 the Retezat Mountains. A previous study identified 30 intact rock glaciers based on geomorphological and ecological criteria
466 (Onaca et al., 2017b). Radar interferometry revealed that 20 rock glaciers exhibit surface displacements exceeding 1 cm yr^{-1} ,
467 while 15 rock glaciers show minimal displacements ($0.3\text{--}1\text{ cm yr}^{-1}$). Among these, eight were previously classified as intact
468 and seven as relict. Notably, four rock glaciers, previously considered geomorphologically relict, now show surface
469 displacements exceeding 1 cm yr^{-1} and are classified as transitional.

470 **5.2. Permafrost occurrence revealed by geophysical and temperature measurements**

471 Geophysical investigations revealed a frozen layer with overall low ice contents beneath a thick active layer ($\sim 5\text{ m}$). Similar
472 results have been reported in other marginal periglacial environments (i.e., Făgăraș Mountains, Pirin Mountains, Italian Carnic
473 Alps) where active layers are often thicker (Onaca et al., 2013; Colucci et al., 2019; Onaca et al., 2020). Due to the rock glacier's

very dry and extremely coarse blocky surface, the ERT data only have limited quality which is also reflected by the high resistivities of $> 200 \text{ k}\Omega\text{m}$ on the rock glacier surface. However, we still assume that the overall resistivity pattern indicates the main structures and is representative for the site, though small-scale anomalies and absolute resistivity values, should be interpreted with cautions.

The BTS measurements revealed very cold surface temperatures ($< -4 \text{ }^{\circ}\text{C}$) across large portions of the rock glaciers, especially within MAs, in the upper sections of the rock glaciers, and along the upper talus slopes. However, not all cold areas exhibited detectable movement in the PSInSAR results. Conversely, warmer surface temperatures ($-2 - -0.3 \text{ }^{\circ}\text{C}$) were also recorded in several areas, indicating the presence of internal ventilation. GST data suggest conditions favourable for permafrost existence, but more notably highlight significant winter ground cooling episodes, likely driven by air advection. Similar patterns were previously observed at Judele, Pietrele, Valea Rea, Galeşu and Pietricelele rock glaciers (Vespremeanu-Stroe et al., 2012; Onaca et al., 2015). Except for Pietrele, all data-logger sites (Galeşu, Judele and Valea Rea) are located within MAs with displacement velocities exceeding 1 cm yr^{-1} . At Pietrele, despite the prevalence of low BTS values, almost no displacement was observed, except in the western part, where minor displacements ($0.3 - 1 \text{ cm yr}^{-1}$) were detected. As Pietrele rock glacier is oriented south-north the LOS orientation likely underestimates displacements on its north facing slopes (Liu et al., 2013). The lack of significant displacement in this rock glacier between 2014 and likely suggests insufficient ice content for permafrost creep, rather than complete ice melt.

5.3. Rock glaciers behaviour in marginal periglacial environment

The rock glaciers in the Southern Carpathians generally move at slower rates than those in other mid-latitude high mountains, where rock glaciers' velocities range from a few centimetres to a few meters per year. But slow-moving rock glaciers were also documented in different periglacial regions (e.g., Pyrenees, Rocky Mountains, northern Norway, Southern Alps of New Zealand, etc.) (Serrano et al., 2010; Brencher et al., 2021; Rouyet et al., 2021; Bertone et al., 2022; Lambiel et al., 2023). In the Retezat Mountains, only 21 % of the inventoried rock glaciers display detectable motion, whereas the rest are considered relict. As in the Uinta Mountains (Brencher et al., 2021), movement is often confined to a limited portion of the landform. An illustrative case in this regard is the Galeşu multi-unit rock glacier, where activity is restricted to the uppermost unit, marked by a younger lobe overlying the main body of the rock glacier. Similar younger lobes were identified in other valleys (e.g., Valea Rea, Pietrele) representing distinct phases of rock glaciers activity, as observed in many other periglacial regions of Europe (e.g. Iceland, European Alps, Cantabrian Mountains, Pyrenees etc.) (Farbrot et al., 2007; Kellerer-Pirklbauer et al., 2008; Steinemann et al., 2020; Amschwand et al., 2021; Oliva et al., 2021; Santos-González et al., 2022).

Additionally, the PSInSAR analysis revealed that the fronts of many rock glaciers in the Retezat Mountains remain stable. Notable examples include Judele (Fig. 11a), Berbecilor (Fig. 11b), Galeşu (Fig. 12a), Păpuşa (Fig. 12c) and Pietricelele (Fig. 12b). Field observations support these findings, revealing no signs of recent activity—such as ploughed grass—despite steep and occasionally unvegetated slopes. These characteristics are typical of climatically inactive rock glaciers (Barsch, 1996), which are often marked by a thick unfrozen surface layer and low ice content (Onaca et al., 2013). Our geophysical measurements revealed a paucity of ice content in the Galeşu rock glacier, insufficient to support permafrost creep. For permafrost creep to occur, frozen conditions must extend to a depth of at least 10-25 m (Cicoira et al., 2021), which does not appear to be the case at Galeşu. Surface displacements at this site are more likely the result of ice-melt-induced subsidence, solifluction, or the tilting and sliding of blocks within the active layer. In contrast, the flow direction of dGNSS markers at Judele and Berbecilor showed consistent movement patterns, consistent with permafrost creep. Further geophysical and dGNSS measurements are needed to better differentiate between these mechanisms in marginal periglacial environments.

Various studies estimate the volumetric ice content in active rock glaciers to range between 40 % and 60 % (Barsch, 1996; Hausmann et al., 2007; Rangecroft et al., 2015). Conversely, for rock glaciers tending towards inactivity, Wagner et al. (2021) propose average ice content as low as 20 %. These values are commonly used to assess the water volume equivalent of ice

content stored in rock glaciers (Wagner et al., 2021; Pandey et al., 2024). Our geophysical investigations reveal even lower values for the volumetric ice content of the Galeşu rock glacier. This finding suggests that the ice content in transitional rock glaciers may be lower than 20 %, emphasising caution when calculating water volume equivalent on a broad scale. Considering the current MAGST of approximately -0.5 °C and assuming a climatic warming of about +1.5 °C since the late 19th century (Allen et al., 2018), these rock glaciers likely had a MAGST around -2 °C during the pre-industrial period. At such low temperatures, widespread permafrost conditions would have been expected, and the presence of deep permafrost cannot be ruled out. However, recent accelerated warming has caused permafrost temperature to rise, especially in ice-poor bedrock, at rates similar to air temperature increases (Noetzli et al., 2024). BTS measurements and GST patterns observed during winter indicate ongoing convective and advective air flow processes that maintain cold ground conditions and support the persistence of ice non-saturated permafrost in the Retezat Mountains. The findings of this study support the coarse-rock glacier hypothesis (Onaca et al., 2015; Popescu et al., 2017), which posits that permafrost occurrence in the Carpathian Mountains is patchy and limited to sites above 2100 m with low solar radiation. In these settings, very coarse rock glaciers with abundant large boulders enhance internal cooling through ventilation processes, such as advection and convection (Wicky and Hauck, 2017; Amschwand et al., 2024), as well as through air stratification (low conductivity) in summer or under thick snow cover.

6. Conclusions

This study leads to the following main conclusions:

- Most rock glaciers in the marginal periglacial environment of the Retezat Mountains are classified as relict, with only 21% categorized as transitional. The median elevation of transitional rock glaciers is 150 m higher than that of relict rock glaciers and their median size is slightly smaller. The PSInSAR methodology enabled the identification of new rock glaciers displaying movements, which were initially classified as relict features.
 - A total of 92 moving areas were delineated within the rock glaciers of the Retezat Mountains, predominantly falling within the slow-velocity classes (0.3 – 1 cm yr⁻¹ and 1-3 cm yr⁻¹). Moving areas exhibiting velocities between 1 and 5 cm yr⁻¹ are typically located above 2100 m in regions with minimal solar radiation income. Higher movement rates are observed in the upper, younger lobes compared to the well-developed lower parts.
 - Long-term ground temperature monitoring from 2012 to 2022 revealed low MAGST values at the observation sites, ranging from -2.3 °C to 0.8 °C. Internal ventilation processes (e.g., advection) occurring throughout the winter significantly contribute to surface cooling and appear to sustain permafrost conditions in coarse debris above 2100 m. BTS measurements further support this, showing very cold ground temperatures beneath thick late-winter snow cover.
 - Geophysical measurements conducted on an intact rock-glacier revealed low ice content (with maximum values of 18%) in its uppermost section. At this site, surface displacements are most likely driven by processes such as ice-melt-induced subsidence, solifluction or blocks sliding. In contrast, the consistent flow of dGNSS markers towards the fronts of the Judele and Berbecilor rock glaciers points to permafrost creep.
- Our findings underscore the value of integrating Sentinel-1 SAR data with extensive field investigation (such as DGPS, geophysical and thermal methods) and where available, complementary remote sensing data (like ALOS-2 PALSAR-2), particularly in regions with slow-moving rock glaciers. This multi-method approach could serve as a benchmark for similar studies in marginal periglacial environments.

Code/Data availability

The deformation data, obtained using PSI, and the temperature data, obtained using GST data loggers and BTS are freely available as a Zendo repository, at <https://zenodo.org/records/14544941>, DOI: 10.5281/zenodo.14544940

For further questions about data processing readers are encouraged to contact the authors.

Author Contribution

The study was conceptualized and managed by AO and FS. AO led the manuscript writing, with contributions from VP, CH, PU, TS and FS. VP, TS, DT, DB and FS contributed to the PSInSAR analysis. FA and IL produced the inventory of moving areas and performed the statistical analysis related to rock glaciers. AO, OB, RP, MV, IL and AVS contributed to the analysis of thermal measurements. CH, BE, SF, RP and AO were involved in conducting and analysing the geophysical measurements. AH and AO provided the GNSS measurements. All authors provided feedback on the final version of the paper.

Competing interests

The authors declare that they have no conflict of interest.

Acknowledgements

This research was funded by the ESA Permafrost_CCI project (grant number 4000123681/18/I-NB), EEA Norway Grants 2014–2021, under project code RO-NO-2019-0415 / contract no. 30/2020, CNCS—UEFISCDI, project number PN-IV-P2-2.1-TE-2023-0603, within PNCDI IV and PNRR-III-C9 2022 - 18, CF 253/29.11.2022, 760055/23.05.2023. We would also like to thank Sabina Calisevici, Adrian C. Ardelean, Patrick Chiroiu, Trond Eiken, Romolus Mălăieștean, Ilie Adrian and Fabian Timofte for support in the fieldwork.

References

- Allen, M. R., Dube, O. P., Solecki, W., Aragón-Durand, F., Cramer, W., Humphreys, S., Kainuma, M., Kala, J., Mahowald, N., Mulugetta, Y., Perez, R., Wairiu, M., and Zickfeld, K.: Framing and Context, In: Global Warming of 1.5 °C, In: An IPCC Special Report on the impacts of global warming of 1.5 °C above pre-industrial levels and related global greenhouse gas emission pathways, in the context of strengthening the global response to the threat of climate change, edited by: Masson-Delmotte, V., Zhai, P., Pörtner, H.-O., Roberts, D., Skea, J., Shukla, P. R., Pirani, A., Moufouma-Okia, W., Péan, C., Pidcock, R., Connors, S., Matthews, J. B. R., Chen, Y., Zhou, X., Gomis, M. I., Lonnoy, E., Maycock, T., Tignor, M., and Waterfield, T., Cambridge University Press, Cambridge, UK and New York, NY, USA, pp. 49–92, <https://doi.org/10.1017/9781009157940.003>, 2018.
- Amschwand, D., Ivy-Ochs, S., Frehner, M., Steinemann, O., Christl, M., and Vockenhuber, C.: Deciphering the evolution of the Bleis Marscha rock glacier (Val d'Err, eastern Switzerland) with cosmogenic nuclide exposure dating, aerial image correlation, and finite element modeling, *The Cryosphere*, 15, 2057–2081, <https://doi.org/10.5194/tc-15-2057-2021>, 2021.
- Amschwand, D., Scherler, M., Hoelzle, M., Krummenacher, B., Haberkorn, A., Kienholz, C., and Gubler, H.: Surface heat fluxes at coarse blocky Murtèl rock glacier (Engadine, eastern Swiss Alps), *The Cryosphere*, 18, 2103–2139 <https://doi.org/10.5194/tc-18-2103-2024>, 2024.
- Archie, G. E.: The electrical resistivity log as an aid in determining some reservoir characteristics, *Petroleum Transactions of American Institute of Mining and Metallurgical Engineers (AIME)*, 146, 54–62, <https://doi.org/10.2118/942054-G>, 1942.
- Barboux, C., Delaloye, R., and Lambiel, C.: Inventorying slope movements in an Alpine environment using DInSAR, *Earth Surf. Processes*, 39, 2087–2099, <https://doi.org/10.1002/esp.3603>, 2014.
- Barsch, D.: *Rockglaciers: Indicators for the Present and Former Geocology in High Mountain Environments*, Springer, Berlin, 331 pp, ISBN 3-540-60742-0, 1996.

Bernhard, L., Sutter, F., Haeberli, W., Keller, F.: Processes of snow/permafrost-interaction at a high-mountain site, Murtél/Corvatsch, Easterns Swiss Alps, in 7th International Conference on Permafrost, Yellowknife, Canada, Collection Nordicana, vol. 57, 35-41, 1998.

Bertone, A., Barboux, C., Bodin, X., Bolch, T., Brardinoni, F., Caduff, R., Christiansen, H. H., Darrow, M. M., Delaloye, R., Etzelmüller, B., Humlum, O., Lambiel, C., Lilleøren, K. S., Mair, V., Pellegrinon, G., Rouyet, L., Ruiz, L., and Strozzi, T.: Incorporating InSAR kinematics into rock glacier inventories: insights from 11 regions worldwide, *The Cryosphere* 16, 2769–2792, <https://doi.org/10.5194/tc-16-2769-2022>, 2022.

Bertone, A., Jones, N., Mair, V., Scotti, R., Strozzi, T., and Brardinoni, F.: A climate-driven, altitudinal transition in rock glacier dynamics detected through integration of geomorphological mapping and synthetic aperture radar interferometry (InSAR)-based kinematics, *The Cryosphere*, 18, 2335–2356, <https://doi.org/10.5194/tc-18-2335-2024>, 2024.

Berzescu, O., Ardelean, F., Urdea, P., Ioniță, A., and Onaca, A.: Thermal Regime Characteristics of Alpine Springs in the Marginal Periglacial Environment of the Southern Carpathians, *Sustainability*, 17(9), 4182, <https://doi.org/10.3390/su17094182>, 2025.

Brencher, G., Handwerger, A.L., and Munroe, J.S.: InSAR-based characterization of rock glacier movement in the Uinta Mountains, Utah, USA, *The Cryosphere*, 15, 4823–4844, <https://doi.org/10.5194/tc-15-4823-2021>, 2021.

Cicoira, A., Beutel, J., Faillettaz, J., and Vieli, A.: Water controls the seasonal rhythm of rock glacier flow, *Earth Planet. Sc. Lett.*, 528, 115844, <https://doi.org/10.1016/j.epsl.2019.115844>, 2019.

Cicoira, A., Marcer, M., Gärtner-Roer, I., Bodin, X., Arenson, L. U., Vieli, A.: A general theory of rock glacier creep based on in-situ and remote sensing observations, *Permafrost Periglac.*, 32, 139-153, <https://doi.org/10.1002/ppp.2090>, 2021.

Colucci, R.R., Forte, E., Žebre, M., Maset, E., Zanettini, C., and Guglielmin, M.: Is that a relict rock glacier?, *Geomorphology*, 330, 177–189, <https://doi.org/10.1016/j.geomorph.2019.02.002>, 2019.

Crosetto, M., Monserrat, O., Cuevas-González, M., Devanthery, N., and Crippa, B.: Persistent Scatterer Interferometry: A review. *ISPRS J. Photogramm.*, 115, 78–89, <http://dx.doi.org/10.1016/j.isprsjprs.2015.10.011>, 2016.

Delaloye, R., and Lambiel, C.: Evidence of winter ascending air circulation throughout talus slopes and rock glaciers situated in the lower belt of alpine discontinuous permafrost (Swiss Alps), *Nor. Geogr. Tidsskr.*, 59, 194-203, <https://doi.org/10.1080/00291950510020673>, 2005.

Delaloye, R., Morard, S., Barboux, C., Abbet, D., Gruber, V., Riedo, M., and Gachet, S.: Rapidly moving rock glaciers in Mattertal. In: *Graf, C. (ed.) Mattertal – ein Tal in Bewegung*. Publikation zur Jahrestagung der Schweizerischen Geomorphologischen Gesellschaft 29. Juni – 1. Juli 2011, St. Niklaus. Birmensdorf, Eidg. Forschungsanstalt WSL. 21-30, 2013.

Eriksen, H. Ø., Rouyet, L., Lauknes, T. R., Berthling, I., Isaksen, K., Hindberg, H., Larsen, Y., and Corner, G. D.: Recent Acceleration of a Rock Glacier Complex, Ádjet, Norway, Documented by 62 Years of Remote Sensing Observations, *Geophys. Res. Lett.*, 45, 8314–8323, <https://doi.org/10.1029/2018GL077605>, 2018.

European Environment Agency (EEA): EGMS Algorithm Theoretical Basis Document (ATBD), Copernicus Land Monitoring Service, (<https://land.copernicus.eu/en/technical-library/egms-algorithm-theoretical-basis-document/@@download/file>), accessed 18 April 2025.

Farbrot, H., Etzelmüller, B., Guðmundsson, Á., Humlum, O., Kellerer-Pirklbauer, A., Eiken, T., and Wangenstein, B.: Rock glaciers and permafrost in Tröllaskagi, Northern Iceland, *Z. Geomorphol.*, 51, 1–16, <https://doi.org/10.1127/0372-8854/2007/0051s2-0001>, 2007.

Haeberli, W.: Die Basis-Temperatur der winterlichen Schneedecke als möglicher Indikator für die Verbreitung von Permafrost in den Alpen, *Zeitschrift für Gletscherkunde und Glazialgeologie*, 9, 221–227, 1973.

Haeberli, W., Hallet, B., Arenson, L., Elconin, R., Humlum, O., Kääb, A., Kaufmann, V., Ladanyi, B., Matsuoka, N., Springman, S., and Mühll, D.V.: Permafrost creep and rock glacier dynamics, *Permafrost Periglac.*, 17, 189–214, <https://doi.org/10.1002/ppp.561>, 2006.

634 Hartl, L., Zieher, T., Bremer, M., Stocker-Waldhuber, M., Zahs, V., Höfle, B., Klug, C., and Cicoira, A.: Multi-sensor monitoring
635 and data integration reveal cyclical destabilization of the Äußeres Hochebenkar rock glacier, *Earth Surf. Dynam.*, 11, 117–147,
636 <https://doi.org/10.5194/esurf-11-117-2023>, 2023.

637 Hauck, C., Böttcher, M., and Maurer, H.: A new model for estimating subsurface ice content based on combined electrical and
638 seismic data sets, *The Cryosphere*, 5, 453–468, <https://doi.org/10.5194/tc-5-453-2011>, 2011.

639 Hausmann, H., Krainer, K., Brückl, E., and Mostler, W.: Internal structure and ice content of Reichenkar rock glacier (Stubai
640 Alps, Austria) assessed by geophysical investigations, *Permafrost Periglac.*, 18, 351–367, <https://doi.org/10.1002/ppp.601>, 2007.

641 Hawker, L., Uhe, P., Paulo, L., Sosa, J., Savage, J., Sampson, C., and Neal, J.: A 30 m global map of elevation with forests and
642 buildings removed. *Environ. Res. Lett.*, 17(2), 2022.

643 Herring, T., Lewkowicz, A. G., Hauck, C., Hilbich, C., Mollaret, C., Oldenborger, G. A., Uhlemann, S., Farzamian, M., Calmels,
644 F., and Scandroglio, R.: Best practices for using electrical resistivity tomography to investigate permafrost, *Permafrost Periglac.*,
645 34, 494–512, <https://doi.org/10.1002/ppp.2207>, 2023.

646 Hoelzle, M.: Permafrost occurrence from BTS measurements and climatic parameters in the eastern Swiss Alps, *Permafrost*
647 *Periglac.*, 3, 143–147, <https://doi.org/10.1002/ppp.3430030212>, 1992.

648 Hoelzle, M., Wegmann, M., and Krummenacher, B.: Miniature temperature dataloggers for mapping and monitoring of
649 permafrost in high mountain areas: First experience from the Swiss Alps, *Permafrost Periglac.*, 10, 113–124,
650 10.1002/(SICI)1099-1530(199904/06)10:23.O.CO;2-A, 1999.

651 Hu, Y., Arenson, L. U., Barboux, C., Bodin, X., Cicoira, A., Delaloye, R., Gärtner-Roer, I., Kääb, A., Kellerer-Pirklbauer, A.,
652 Lambiel, C., Liu, L., Pellet, C., Rouyet, L., Schoeneich, P., Seier, G., and Strozzi, T.: Rock glacier velocity: An Essential Climate
653 Variable Quantity for Permafrost, *Rev. Geophys.*, 63(1), e2024RG000847, <https://doi.org/10.1029/2024RG000847>, 2025.

654 Ishikawa, M., Fukui, K., Aoyama, M., Ikeda, A., Sawada, Y., and Matsuoka, N.: Mountain permafrost in Japan: Distribution,
655 landforms and thermal regimes, *Z. Geomorphol. Supp.*, 130, 99–116, 2003.

656 Kääb, A., Frauenfelder, R. and Roer, I.: On the response of rockglacier creep to surface temperature increase, *Glob. Planet.*
657 *Change*, 56, 172–187, <https://doi.org/10.1016/j.gloplacha.2006.07.005>, 2007.

658 Kääb, A., Strozzi, T., Bolch, T., Caduff, R., Trefall, H., Stoffel, M., and Kokarev, A.: Inventory and changes of rock glacier
659 creep speeds in Ile Alatau and Kungöy Ala-Too, northern Tien Shan, since the 1950s, *The Cryosphere*, 15, 927–949,
660 <https://doi.org/10.5194/tc-15-927-2021>, 2021.

661 Kääb, A. and Røste, A.: Rock glaciers across the United States predominantly accelerate coincident with rise in air temperatures,
662 *Nat. Commun.*, 15, 7581, <https://doi.org/10.1038/s41467-024-52093-z>, 2024.

663 Kellerer-Pirklbauer, A., Wangenstein, B., Farbrot, H., and Etzelmüller, B.: Relative surface age-dating of rock glacier systems
664 near Hólar in Hjaltadalur, northern Iceland, *J. Quaternary Sci.*, 23, 137–151, <https://doi.org/10.1002/jqs.1117>, 2008.

665 Kellerer-Pirklbauer, A.: Long-term monitoring of sporadic permafrost at the eastern margin of the European Alps (Hochreichart,
666 Seckauer Tauern range, Austria), *Permafrost Periglac.*, 30, 260–277, <https://doi.org/10.1002/ppp.2021>, 2019.

667 Kellerer-Pirklbauer, A., Lieb, G.K., Kaufmann, V.: Rock Glaciers in the Austrian Alps: A General Overview with a Special
668 Focus on Dösen Rock Glacier, Hohe Tauern Range. In: Embleton-Hamann, C. (eds) *Landscapes and Landforms of Austria*.
669 *World Geomorphological Landscapes*. Springer, Cham, pp. 393–406, https://doi.org/10.1007/978-3-030-92815-5_27, 2022.

670 Kellerer-Pirklbauer, A., Bodin, X., Delaloye, R., Lambiel, C., Gärtner-Roer, I., Bonnefoy-Demongeot, M., Carturan, L., Damm,
671 B., Eulenstein, J., Fischer, A., Hartl, L., Ikeda, A., Kaufmann, V., Krainer, K., Matsuoka, N., Di Cella, U.M., Noetzi, J., Seppi,
672 R., Scapozza, C., Schoeneich, P., Stocker-Waldhuber, M., Thibert, E., and Zumiani, M.: Acceleration and interannual variability
673 of creep rates in mountain permafrost landforms (rock glacier velocities) in the European Alps in 1995–2022, *Environ. Res.*
674 *Lett.*, 19, 034022, <https://doi.org/10.1088/1748-9326/ad25a4>, 2024.

675 Kenner, R., Pruessner, L., Beutel, J., Limpach, P., and Phillips, M.: How rock glacier hydrology, deformation velocities and
676 ground temperatures interact: Examples from the Swiss Alps, *Permafrost Periglac.*, 31, 3–14, <https://doi.org/10.1002/ppp.2023>,
677 2020.

678 LAKI II MNT: Agentia Nationala de Cadastru si Publicitate Imobiliara: Land Administration Knowledge Improvement,
679 available online: geoportal.ancpi.ro last acces: 01.09.2024, 2024.

680 Lambiel, C., Strozzi, T., Paillex, N., Vivero, S., and Jones, N.: Inventory and kinematics of active and transitional rock glaciers
681 in the Southern Alps of New Zealand from Sentinel-1 InSAR, *Arctic Antarct. Alp. Res.*, 55, 2183999,
682 <https://doi.org/10.1080/15230430.2023.2183999>, 2023.

683 Lilleøren, K.S., Etzelmüller, B., Rouyet, L., Eiken, T., Slinde, G., and Hilbich, C.: Transitional rock glaciers at sea level in
684 northern Norway, *Earth Surf. Dynam.*, 10, 975–996, <https://doi.org/10.5194/esurf-10-975-2022>, 2022.

685 Liu, L., Millar, C.I., Westfall, R.D., and Zebker, H.A.: Surface motion of active rock glaciers in the Sierra Nevada, California,
686 USA: Inventory and a case study using InSAR, *The Cryosphere*, 7, 1109–1119, <https://doi.org/10.5194/tc-7-1109-2013>, 2013.

687 Marcer, M., Cicoira, A., Cusicanqui, D., Bodin, X., Echelard, T., Obregon, R., and Schoeneich, P.: Rock glaciers throughout
688 the French Alps accelerated and destabilised since 1990 as air temperatures increased, *Commun. Earth Environ.*, 2,
689 <https://doi.org/10.1038/s43247-021-00150-6>, 2021.

690 Mollaret, C., Wagner, F.M., Hilbich, C., Scapozza, C., and Hauck, C.: Petrophysical Joint Inversion Applied to Alpine
691 Permafrost Field Sites to Image Subsurface Ice, Water, Air, and Rock Contents, *Front. Earth Sci.*, 8, 85,
692 <https://doi.org/10.3389/feart.2020.00085>, 2020.

693 Necsoiu, M., Onaca, A., Wigginton, S., and Urdea, P.: Rock glacier dynamics in Southern Carpathian Mountains from high-
694 resolution optical and multi-temporal SAR satellite imagery, *Remote Sens. Environ.*, 177, 21–36,
695 <https://doi.org/10.1016/j.rse.2016.02.025>, 2016.

696 Oliva, M., Fernandes, M., Palacios, D., Fernández-Fernández, J.M., Schimmelpfennig, I., Antoniades, D., Aumaître, G., Bourlès,
697 D., and Keddadouche, K.: Rapid deglaciation during the Bølling-Allerød Interstadial in the Central Pyrenees and associated
698 glacial and periglacial landforms, *Geomorphology*, 385, 107735, <https://doi.org/10.1016/j.geomorph.2021.107735>, 2021.

699 Onaca, A.L., Urdea, P., and Ardelean, A.C.: Internal structure and permafrost characteristics of the rock glaciers of Southern
700 Carpathians (Romania) assessed by geoelectrical soundings and thermal monitoring, *Geogr. Ann. A.*, 95, 249–266,
701 <https://doi.org/10.1111/geoa.12014>, 2013.

702 Onaca, A., Ardelean, A.C., Urdea, P., Ardelean, F., and Sirbu, F.: Detection of mountain permafrost by combining conventional
703 geophysical methods and thermal monitoring in the Retezat Mountains, Romania, *Cold Reg. Sci. Technol.*, 119, 111–123,
704 <https://doi.org/10.1016/j.coldregions.2015.08.001>, 2015.

705 Onaca, A., Urdea, P., Ardelean, A.C., Șerban, R., and Ardelean, F.: Present-day periglacial processes in the alpine zone, in:
706 *Landform Dynamics and Evolution in Romania*, edited by: Rădoane, M., Vespremeanu-Stroe, A., Springer Geography, 147-
707 176, 2017a.

708 Onaca, A., Ardelean, F., Urdea, P., and Magori, B.: Southern Carpathian rock glaciers: Inventory, distribution and environmental
709 controlling factors, *Geomorphology*, 293, 391-404, <http://dx.doi.org/10.1016/j.geomorph.2016.03.032>, 2017b.

710 Onaca, A., Ardelean, F., Ardelean, A., Magori, B., Sirbu, F., Voiculescu, M., and Gachev, E.: Assessment of permafrost
711 conditions in the highest mountains of the Balkan Peninsula, *Catena*, 185, 104288, <https://doi.org/10.1016/j.catena.2019.104288>,
712 2020.

713 Noetzli, J., Isaksen, K., Christiansen, H., Delaloye, R., Etzelmüller, B., Farinotti, D., Gallemann, T., Guglielmin, M., Hauck, C.,
714 Hilbich, C., Hoelzle, M., Lambiel, C., Magnin, F., Oliva, M., Paro, L., Pogliotti, P., Riedl, C., Schoeneich, P., Valt, M., Vieli,
715 M., and Philips, M.: Enhanced warming of European mountain permafrost in the early 21st century, *Nat. Commun.*, 15,
716 10508, <https://doi.org/10.1038/s41467-024-54831-9>, 2024.

717 Pavelescu, L.: Studiu geologic și petrografic al regiunii centrale și de sud-est a Munților Retezat [Geological and petrographic
718 study of the central and south-eastern region of the Retezat Mountains], *AIGR*, XXV, 119-210, 1953.

Pandey, P., Nawaz Ali, S., Subhasmita Das, S., and Ataullah Raza Khan, M.: Rock glaciers of the semi-arid northwestern Himalayas: distribution, characteristics, and hydrological significance, *Catena*, 238, 107845, <https://doi.org/10.1016/j.catena.2024.107845>, 2024.

Pellet, C., Bodin, X., Cusicanqui, D., Delaloye, R., Kääb, A., Kaufmann, V., Thibert, E., Vivero, S., and Kellerer-Pirklbauer, A.: Rock glacier velocity. In: State of the Climate in 2023, *Bull. Am. Meteorol. Soc.*, 105, 44–46, <https://doi.org/10.1175/2024BAMSStateoftheClimate.1>, 2024.

Poncoş, V., Stanciu, I., Teleagă, D., Maţenco, L., Bozsó, I., Szakács, A., Birtas, D., Toma, Ş.A., Stănică, A., and Rădulescu, V.: An Integrated Platform for Ground-Motion Mapping, Local to Regional Scale; Examples from SE Europe, *Remote Sens-Basel*, 14, 1046, <https://doi.org/10.3390/rs14041046>, 2022.

Popescu, R., Vespremeanu-Stroe, A., Onaca, A., and Cruceru, N.: Permafrost research in the granitic massifs of Southern Carpathians (Parâng Mountains), *Z. für Geomorphol*, 59(1), 1–20, doi.org/10.1127/0372-8854/2014/0145, 2015.

Popescu, R., Onaca, A., Urdea, P., and Vespremeanu-Stroe, A.: Spatial Distribution and Main Characteristics of Alpine Permafrost from Southern Carpathians, Romania, In Rădoane, M., Vespremeanu-Stroe, A. (Eds.), *Landform dynamics and evolution in Romania*, Springer, 117–146, DOI: 10.1007/978-3-319-32589-7_6, 2017.

Popescu, R., Filhol, S., Etzelmüller, B., Vasile, M., Pleşoianu, A., Virghileanu, M., Onaca, A., Şandric, I., Săvulescu, I., Cruceru, N., Vespremeanu-Stroe, A., Westermann, S., Sîrbu, F., Mihai, B., Nedelea, A., and Gascoin, S.: Permafrost Distribution in the Southern Carpathians, Romania, Derived From Machine Learning Modeling, *Permafrost Periglac.*, 35, 243–261, <https://doi.org/10.1002/ppp.2232>, 2024.

Rangecroft, S., Harrison, S., and Anderson, K.: Rock glaciers as water stores in the Bolivian Andes: An assessment of their hydrological importance, *Arct. Antarct. Alp. Res.*, 47, 89–98, <https://doi.org/10.1657/AAAR0014-029>, 2015.

RGIK: Guidelines for inventorying rock glaciers: baseline and practical concepts (version 1.0). IPA Action Group Rock glacier inventories and kinematics, 25, DOI:10.51363/unifr.srr.2023.002, 2023a.

RGIK: InSAR-based kinematic attribute in rock glacier inventories. Practical InSAR Guidelines (version 4.0., 31.05.2023), IPA Action Group Rock Glacier Inventories and Kinematics (RGIK), 33 pp, www.rgik.org, 2023b.

Roer, I., Haeberli, W., Avian, M., Kaufmann, V., Delaloye, R., Lambiel, C., and Kääb, A.: Observations and considerations on destabilizing active rock glaciers in the European Alps, in: *Proc. Ninth Int. Conf. on Permafrost*, Fairbanks, Alaska, 29 June–3 July 2008, Kane, D. L. and Hinkel, K. M. (Eds.), Institute of Northern Engineering, University of Alaska, pp. 1505–1510, 2008.

Rouyet, L., Lilleoren, K.S., Boehme, M., Vick, L.M., Delaloye, R., Etzelmüller, B., Lauknes, T.R., Larsen, Y., and Blikra, L.H.: Regional Morpho-Kinematic Inventory of Slope Movements in Northern Norway, *Front. Earth Sci.* 9, 681088, <https://doi.org/10.3389/feart.2021.681088>, 2021.

Rucci, A., Ferretti, A., Monti Guarnieri, A., and Rocca, F.: Sentinel 1 SAR interferometry applications: The outlook for sub millimeter measurements, *Remote Sens. Environ.*, 120, 156–163, <https://doi.org/10.1016/j.rse.2011.09.030>, 2012.

Rücker, C., Günther, T., and Wagner, F.M.: pyGIMLi: An open-source library for modelling and inversion in geophysics, *Comput. Geosci.*, 109, 106–123, <https://doi.org/10.1016/j.cageo.2017.07.011>, 2017.

Ruszkiczay-Rüdiger, Z., Kern, Z., Urdea, P., Madarász, B., Braucher, R., and ASTER Team: Limited glacial erosion during the last glaciation in mid-latitude cirques (Retezat Mts, Southern Carpathians, Romania), *Geomorphology*, 384, 107719, <https://doi.org/10.1016/j.geomorph.2021.107719>, 2021.

Sandmeier, K.-J.: REFLEXW Version 9.1.3. Windows™ XP/7/8/10-program for the processing of seismic, acoustic or electromagnetic reflection, refraction and transmission data, 2020.

Santos-González, J., González-Gutiérrez, R.B., Redondo-Vega, J.M., Gómez-Villar, A., Jomelli, V., Fernández-Fernández, J.M., Andrés, N., García-Ruiz, J.M., Peña-Pérez, S.A., Melón-Nava, A., Oliva, M., Álvarez-Martínez, J., Charton, J., ASTER Team, and Palacios, D.: The origin and collapse of rock glaciers during the Bølling-Allerød interstadial: A new study case from the Cantabrian Mountains (Spain), *Geomorphology*, 401, 108112, <https://doi.org/10.1016/j.geomorph.2022.108112>, 2022.

762 Sattler, K., Anderson, B., Mackintosh, A., Norton, K., and de Róiste, M.: Estimating permafrost distribution in the maritime
763 Southern Alps, New Zealand, based on climatic conditions at rock glacier sites, *Front. Earth Sci.*, 4, 4,
764 <https://doi.org/10.3389/feart.2016.00004>, 2016.

765 Schoeneich, P.: Guide lines for monitoring GST – Ground surface temperature, PERMANET project, Version 3 – 2.2.2011,
766 <https://www.permanet-alpinespace.eu/archive/pdf/GST.pdf>, 2011, accessed 20 April 2025.

767 Serrano, E., de Sanjosé, J.J., and González-Trueba, J.J.: Rock glacier dynamics in marginal periglacial environments, *Earth Surf.*
768 *Proc. Land.*, 35, 1302–1314, <https://doi.org/10.1002/esp.1972>, 2010.

769 Steinemann, O., Reitner, J.M., Ivy-Ochs, S., Christl, M., and Synal, H.-A.: Tracking rockglacier evolution in the Eastern Alps
770 from the Lateglacial to the early Holocene, *Quaternary Sci. Rev.*, 241, 106424, <https://doi.org/10.1016/j.quascirev.2020.106424>,
771 2020.

772 Stiegler, C., Rode, M., Sass, O., and Otto, J.C.: An Undercooled Scree Slope Detected by Geophysical Investigations in Sporadic
773 Permafrost below 1000 M ASL, Central Austria, *Permafrost Periglac.*, 25, 194–207, <https://doi.org/10.1002/ppp.1813>, 2014.

774 Strozzi, T., Caduff, R., Jones, N., Barboux, C., Delaloye, R., Bodin, X., Käab, A., Mätzler, E., and Schrott, L.: Monitoring rock
775 glacier kinematics with satellite synthetic aperture radar, *Remote Sens-Basel.*, 12, 559, <https://doi.org/10.3390/rs12030559>,
776 2020.

777 Timur, A.: Velocity of compressional waves in porous media at permafrost temperatures, *Geophysics*, 33, 584–595,
778 <https://doi.org/10.1190/1.1439954>, 1968.

779 Urdea, P.: Permafrost and periglacial forms in the Romanian Carpathians, in: 6th International Conference on Permafrost, South
780 China University of Technology, Beijing, China, 631–637, 1993.

781 Urdea, P.: Munții Retezat, *Studiu geomorfologic [Retezat Mountains. A geomorphological study]*, Academiei, București, 272
782 pp, ISBN 973-27-0767-4, 2000.

783 Vespremeanu-Stroe, A., Urdea, P., Popescu, R., and Vasile, M.: Rock Glacier Activity in the Retezat Mountains, Southern
784 Carpathians, Romania, *Permafrost Periglac.*, 23, 127–137, <https://doi.org/10.1002/ppp.1736>, 2012.

785 Vonder Mühll, D., Hauck, C., and Gubler, H.: Mapping of mountain permafrost using geophysical methods, *Prog. Phys. Geog.*,
786 26, 643–660, <https://doi.org/10.1191/0309133302pp356ra>, 2002.

787 Wagner, F.M., Mollaret, C., Günther, T., Kemna, A., and Hauck, C.: Quantitative imaging of water, ice and air in permafrost
788 systems through petrophysical joint inversion of seismic refraction and electrical resistivity data, *Geophys. J. Int.*, 219, 1866–
789 1875, <https://doi.org/10.1093/gji/ggz402>, 2019.

790 Wagner, T., Seelig, S., Helfricht, K., Fischer, A., Avian, M., Krainer, K., and Winkler, G.: Assessment of liquid and solid water
791 storage in rock glaciers versus glacier ice in the Austrian Alps, *Sci. Total Environ.*, 800, 149593,
792 <https://doi.org/10.1016/j.scitotenv.2021.149593>, 2021.

793 Wicky, J. and Hauck, C.: Numerical modelling of convective heat transport by air flow in permafrost talus slopes, *The*
794 *Cryosphere*, 11, 1311–1325, <https://doi.org/10.5194/tc-11-1311-2017>, 2017.

795 Wirz, V., Gruber, S., Purves, R.S., Beutel, J., Gärtner-Roer, I., Gubler, S., and Vieli, A.: Short-term velocity variations at three
796 rock glaciers and their relationship with meteorological conditions, *Earth Surf. Dynam.*, 4, 103–123,
797 <https://doi.org/10.5194/esurf-4-103-2016>, 2016.

798 Yu, J., Meng, X., Yan, B., Xu, B., Fan, Q., and Xie, Y.: Global Navigation Satellite System-based positioning technology for
799 structural health monitoring: a review, *Struct. Control. Hlth.*, 27, 2467, <https://doi.org/10.1002/stc.2467>, 2020.